J Comput Neurosci (2009) 26:339–368
DOI 10.1007/s10827-008-0116-4

A kinetic theory approach to capturing interneuronal correlation: the feed-forward case

Chin-Yueh Liu · Duane Q. Nykamp

Received: 9 June 2008 / Revised: 19 September 2008 / Accepted: 24 September 2008 / Published online: 6 November 2008

Abstract We present an approach for using kinetic theory to capture first and second order statistics of neuronal activity. We coarse grain neuronal networks into populations of neurons and calculate the population average firing rate and output cross-correlation in response to time varying correlated input. We derive coupling equations for the populations based on first and second order statistics of the network connectivity. This coupling scheme is based on the hypothesis that second order statistics of the network connectivity are sufficient to determine second order statistics of neuronal activity. We implement a kinetic theory representation of a simple feed-forward network and demonstrate that the kinetic theory model captures key aspects of the emergence and propagation of correlations in the network, as long as the correlations do not become too strong. By analyzing the correlated activity of feed-forward networks with a variety of connectivity patterns, we provide evidence supporting our hypothesis of the sufficiency of second order connectivity statistics.

Keywords Population density · Neuronal network · Synchrony · Syn-fire chain · Connectivity patterns · Maximum entropy

Action Editor: Carson C. Chow

C.-Y. Liu · D. Q. Nykamp (✉)
School of Mathematics, University of Minnesota,
206 Church St., Minneapolis, MN 55455, USA
e-mail: nykamp@math.umn.edu

1 Introduction

Understanding how the brain's neuronal networks perform computations remains a difficult challenge. The interaction of large populations of neurons leads to a complex repertoire of high-dimensional activity patterns that is difficult to analyze. One possibility to reduce the dimensionality and complexity of such networks is to ignore high order interactions among neurons and simply analyze the consequences of low order interactions. Stopping at second order interactions may provide a good description, as recent evidence suggests that pairwise firing statistics among neurons may be sufficient to capture most of the higher order firing patterns (Schneidman et al. 2006; Shlens et al. 2006; Tang et al. 2008; Yu et al. 2008).

We present a kinetic theory approach that is designed to capture the second order interactions among neurons. Kinetic theory approaches have been used to model gases and plasmas, where one uses moment closure approximations to derive equations for lower order statistics of a system of particles (Ichimaru 1973; Nicholson 1992). We implement a similar approach to track the second order statistics among neurons in a population while explicitly neglecting third and higher order statistics.

1.1 Motivation for approach

To understand the behavior of a neuronal network, one may be interested in uncovering the relationship between the network structure and the behavior. Modeling neuronal networks is challenging as the set of possible connectivity combinations is enormous and we do not have experimental methods to determine the

fine details of connectivity. Even if we could exactly determine the connectivity of the network, one would still be faced with the challenge of determining what features of the network underlie the behavior of interest. As the exact connectivity of a given network within the brain may vary widely among individuals while the behavior of interest is maintained, all the details of the connectivity may not be important for the behavior. One would like a method to distill the connectivity down to its key features and to study how these features influence the behavior.

Recent experimental results suggest an approach that may be promising. A number of labs have provided evidence that the second order statistics of interneuronal firing patterns may be sufficient to describe a large fraction of the higher order firing patterns (Schneidman et al. 2006; Shlens et al. 2006; Tang et al. 2008; Yu et al. 2008). In a similar manner, we hypothesize that the second order statistics of connectivity patterns may be sufficient to explain a large fraction of the behavior of the brain's neuronal networks. If the second order connectivity statistics were sufficient to explain the second order statistics of firing patterns, then the above experimental results suggest they should be sufficient to explain a large fraction of the higher order firing patterns of the brain's neuronal networks.

If second order connectivity statistics do capture much of the relevant network behavior, then one can greatly simplify the space of connectivity patterns, parameterizing them by just their second order statistics. One could attempt to understand network behavior by exploring the consequences of these second order connectivity statistics. To do so, one would like a method to analyze network behavior as a function of just the second order connectivity statistics while imposing as little as possible additional structure on the higher order connectivity patterns.

One approach is to use kinetic theory to develop tools to study second order statistics of the activity and connectivity of neuronal networks. With kinetic theory, one can explicitly ignore higher order statistics and simply model second order distributions among the variables of interest. Then, one can use maximum entropy methods (Jaynes 1957) to infer higher order distributions with minimal structure.

1.2 Principles underlying our kinetic theory implementation

Our kinetic theory implementation begins with a coarse graining step where we group neurons into populations (see left two panels of Fig. 1). Within each population, we will assume the neurons have identical properties and identical statistics, so this step clearly leads to a loss of detail. For each population, we will track the distribution of neurons over state space with a density function that we call a population density function (Nykamp and Tranchina 2000). However, unlike previous approaches, we will not assume that the neurons within a population are independent. Instead, we explicitly represent the joint distribution of any pair of neurons with the population density $\rho(\mathbf{x}_1, \mathbf{x}_2, t)$, where each vector $\mathbf{x}_i$ represents a value of the state variables for a single neuron. Roughly speaking, the quantity $\rho(\mathbf{x}_1, \mathbf{x}_2, t)d\mathbf{x}_1 d\mathbf{x}_2$ represents the probability that the state variables $\mathbf{X}_i(t)$ and $\mathbf{X}_j(t)$ at time t of two neurons in the population are near the values $\mathbf{x}_1$ and $\mathbf{x}_2$. Since we assume this holds for any pair of neurons, the population density $\rho(\mathbf{x}_1, \mathbf{x}_2, t)$ clearly must be symmetric in $\mathbf{x}_1$ and $\mathbf{x}_2$.

Once we form a population density $\rho_j(\mathbf{x}_1, \mathbf{x}_2, t)$ for each coarse-grained population j, we need to determine the second order statistics for the connectivity of the

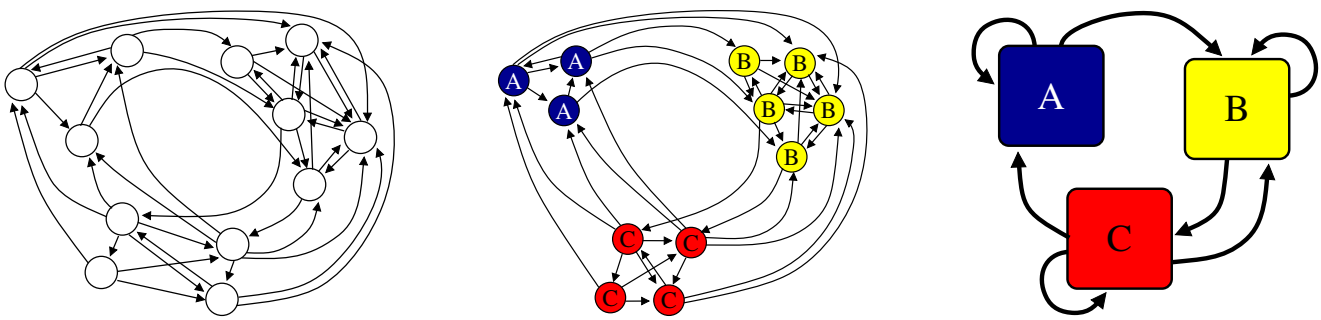

Fig. 1 Schematic illustration of the procedure for forming kinetic theory approximations of neuronal networks. Starting with a neuronal network (*left*), we group neurons into populations, which we indicate by letters (*middle*). For each population, we represent first and second order statistics of neuronal activity with population density functions (*right*). The coupling among the population density functions is based on first and second order statistics of the original network connectivity

populations. For our kinetic theory implementation, we will use the following two statistics (see Fig. 2):

1. W^1_{jk}, the average number of neurons from population j that project onto a single neuron in population k (a first order statistic), and
2. W^2_{jk}, the average number of neurons from population j that simultaneously project onto a pair of neurons in population k (a second order statistic).

In presenting the results, we will typically use the ratio $\beta_{jk} = W^2_{jk}/W^1_{jk}$ for the second order statistic. We refer to β_{jk} as the fraction of shared input parameter.

To derive coupling equations for the network of population densities, one must develop a method to capture the effect of the connectivity statistics on the interactions among the population density functions. Then, one can complete the simplification of the original network (e.g., left of Fig. 1) into a kinetic theory network of interacting population densities (e.g., right of Fig. 1).

The goal is to develop a kinetic theory network approach where the population density functions capture the second order statistics in the neuronal activity and the interaction terms capture the second order statistics of the connectivity. Such a tool could be used to explore the consequences of connectivity in a setting where both the connectivity and the neuronal activity are highly simplified and lower dimensional (Nirenberg and Victor 2007) due to the neglect of higher order statistics. This simplified framework may facilitate exploration of the key features of connectivity that underlie network behavior.

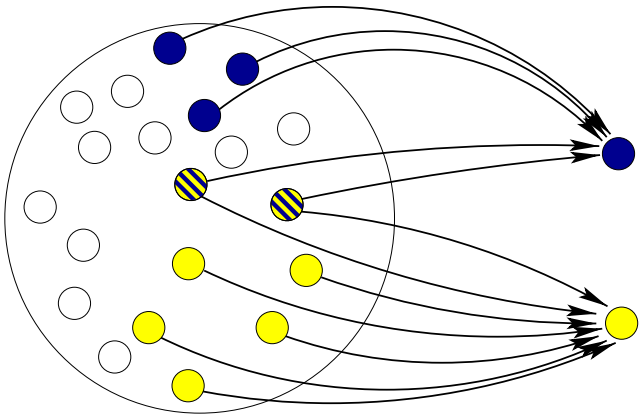

Fig. 2 Illustration of the second order statistics of connectivity used in our kinetic theory approach. We consider the connections from a presynaptic population (*left group*) onto any pair of neurons from a postsynaptic population (*right*). The first order statistic W^1 is the expected number of neurons from the presynaptic population that project to a single postsynaptic neuron (six in this illustration). The second order statistic W^2 is the expected number of presynaptic neurons that project to both postsynaptic neurons (two in this case). The fraction of shared inputs parameter is their ratio $\beta = W^2/W^1$ (which is 1/3 in this case)

In this paper, we have more modest goals than alluded to above. As an initial test of the potential of this approach, we develop in Section 2 a kinetic theory approach for modeling the emergence and propagation of correlations through excitatory feed-forward networks of integrate-and-fire neurons. We gauge the performance of this approach as well as test our hypothesis of the sufficiency of second order connectivity statistics in Section 3. We discuss the successes and failures of this implementation in Section 4.

2 Derivation of feed-forward kinetic theory model

As an initial test of our kinetic theory approach to capturing second order statistics, we seek to develop a second order kinetic theory description of excitatory feed-forward networks of integrate-and-fire neurons. Feed-forward networks are an ideal test system for this approach for a few reasons. First, we study feed-forward networks that are naturally divided into layers, and we can group all neurons of a layer into a single population with little adverse effect of the coarse-graining. Second, neurons within each population do not interact, so one can derive a simplified kinetic theory description. Third, it is well-known that correlations emerge and propagate through feed-forward networks (Diesmann et al. 1999), and the feed-forward networks will be a good test case to see if the kinetic theory model correctly captures this build-up of correlation.

2.1 The integrate-and-fire model

To keep the kinetic theory equations as simple as possible, we base our implementation on a simplified integrate-and-fire model of neuronal dynamics. We let $V_j(t)$ be the voltage of neuron j at time t and let the voltage evolve according to the stochastic differential equation

$$\frac{\mathrm{d}V_j}{\mathrm{d}t} = \frac{E_\mathrm{r} - V_j}{\tau} + \sum_i A^i_j \delta\big(t - T^i_j\big), \tag{1}$$

where τ is the membrane time constant, E_r is the resting potential, and $\delta(t)$ is the Dirac delta function. At the times T^i_j of excitatory synaptic input, the voltage jumps up by the amount A^i_j, which is a random variable with probability density function $f_A(x)$. We define spike times t_sp as those times when $V(t)$ crosses the firing

threshold $v_{\rm th}$, and we immediately reset the voltage to $V(t_{\rm sp}^+) = v_{\rm reset}$, where $v_{\rm reset} < E_{\rm r} < v_{\rm th}$. We use this model because the state of the neuron is described by just the single state variable $V(t)$.

We assume the arrival times T_j^i of the input for each neuron j are given by a modulated Poisson process, where the rate is identical for each neuron in a given population. In departure from previous kinetic theory implementations, we allow the inputs to any pair of neurons in the population to be correlated, though for simplicity, we only model instantaneous correlations in the input. We assume that the inputs to any pair of neurons are given by independent Poisson processes to each neuron at rate $\nu_{\rm ind}(t)$ combined with synchronous input to both neurons from a third independent Poisson process at rate $\nu_{\rm syn}(t)$. This correlated input will create correlations among the neurons in the population, which we will represent with a population density function. A schematic of the random walk exhibited by a pair of neurons with this input is shown in Fig. 3. The

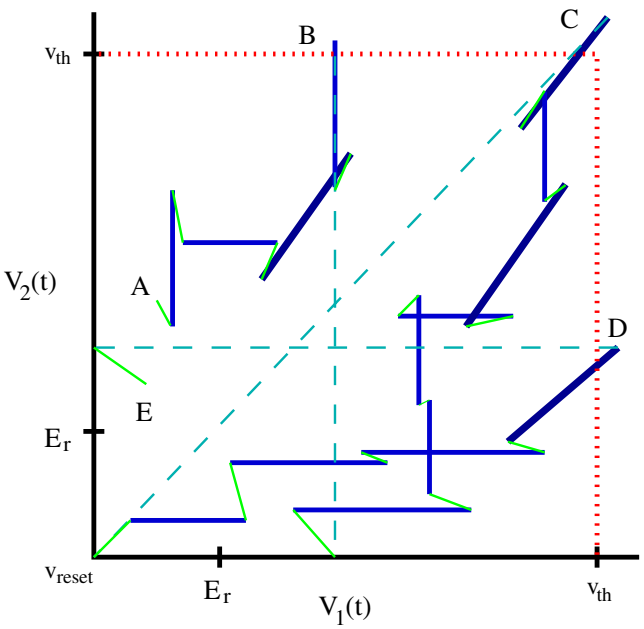

Fig. 3 Schematic of random walk of the voltages of a pair of neurons. The neuron voltages $(V_1(t), V_2(t))$ start at the point indicated by A. Neuron 2 fires alone at B, the neurons fire synchronously at C, neuron 1 fires alone at D, and the voltages end at E. Synchronous input jumps are indicated by the *thick diagonal lines* and independent input jumps are indicated by *horizontal or vertical solid lines*. Voltage decay toward $(E_{\rm r}, E_{\rm r})$ in between inputs is indicated by the *thin diagonal lines*. After one or more neurons fire by crossing the threshold $v_{\rm th}$ (*dotted line*), the voltage is reset to $v_{\rm reset}$, as indicated by the *dashed lines*. For a large population of neurons, the voltages $(V_j(t), V_k(t))$ of each neuron pair can be viewed as following such a random walk, and the population density $\rho(v_1, v_2, t)$ captures the fraction of neuron pairs in the population with voltages $(V_j(t), V_k(t))$ around (v_1, v_2)

random walk includes the decay toward $E_{\rm r}$ in between inputs as well as the voltage reset to $v_{\rm reset}$ after crossing the threshold $v_{\rm th}$.

2.2 The kinetic theory equations

To form a population density function, we assume all neurons in the population are identical and that every pair has the same second order statistics. We represent the second order statistics among the state variables $V_j(t)$ by the population density function $\rho(v_1, v_2, t)$, defined by

$$\int_\Omega \rho(v_1, v_2, t)\mathrm{d}v_1\mathrm{d}v_2 = \Pr\big((V_j(t), V_k(t)) \in \Omega\big),$$

where Ω is any region in the v_1-v_2 phase plane and $V_j(t)$ and $V_k(t)$ are the voltages of any two neurons in the population. For simplicity, we will refer to the voltages as $V_1(t)$ and $V_2(t)$. For a large population of neurons, one can view $\int_\Omega \rho(v_1, v_2, t)\mathrm{d}v_1\mathrm{d}v_2$ as the fraction of neuron pairs with voltages in the region Ω.

Since the input to a pair of neurons is a correlated Poisson process, the history of the synaptic input does not influence future evolution of the voltage and the evolution of the voltage pair $(V_1(t), V_2(t))$ is a Markov process. The evolution of $(V_1(t), V_2(t))$ contains the deterministic evolution of the voltages toward $E_{\rm r}$ due to the leakage term from Eq. (1), and it contains the jump processes due to independent and synchronous inputs, as well as reset to $v_{\rm reset}$ after spiking. We can write down the differential Chapman–Kolmogorov equation (Gardiner 2004) to describe these processes as follows:

$$\begin{aligned}
\frac{\partial\rho}{\partial t}(v_1, v_2, t) = {} & \frac{1}{\tau}\frac{\partial}{\partial v_1}\left[(v_1 - E_{\rm r})\rho(v_1, v_2, t)\right] \\
& + \frac{1}{\tau}\frac{\partial}{\partial v_2}\left[(v_2 - E_{\rm r})\rho(v_1, v_2, t)\right] \\
& + \nu_{\rm ind}(t)\left[\int_{v_{\rm reset}}^{v_1} f_A(v_1 - \theta_1)\rho(\theta_1, v_2, t)\mathrm{d}\theta_1 \right. \\
& \qquad \left. - \rho(v_1, v_2, t)\right] \\
& + \nu_{\rm ind}(t)\left[\int_{v_{\rm reset}}^{v_2} f_A(v_2 - \theta_2)\rho(v_1, \theta_2, t)\mathrm{d}\theta_2 \right. \\
& \qquad \left. - \rho(v_1, v_2, t)\right] \\
& + \nu_{\rm syn}(t)\left[\int_{v_{\rm reset}}^{v_1}\int_{v_{\rm reset}}^{v_2} f_A(v_1 - \theta_1)\, f_A(v_2 - \theta_2) \right. \\
& \qquad \left. \times \rho(\theta_1, \theta_2, t)\mathrm{d}\theta_2\mathrm{d}\theta_1 - \rho(v_1, v_2, t)\right] \\
& + \delta(v_1 - v_{\rm reset})J_{{\rm reset},1}(v_2, t) \\
& + \delta(v_2 - v_{\rm reset})J_{{\rm reset},2}(v_1, t) \\
& + \delta(v_1 - v_{\rm reset})\delta(v_2 - v_{\rm reset})J_{{\rm reset},3}(t). \quad (2)
\end{aligned}$$

The first two lines of Eq. (2) contain the advection terms due to the leak current of Eq. (1) that draws each voltage toward the resting potential E_r. The third and fourth lines describe the jumps due to independent input to neuron 1. The integral contains the contribution to $\rho(v_1, v_2, t)$ due to a neuron with voltage $V_1(t) = \theta_1$ receiving an input of size $v_1 - \theta_1$ so that it lands at $V_1(t) = v_1$. The second term is the loss of probability at $\rho(v_1, v_2, t)$ due to neurons with voltage $V_1(t) = v_1$ receiving an independent input and jumping to a higher voltage. The fifth and sixth lines of Eq. (2) are the symmetric terms for independent input to neuron 2. The seventh and eighth lines describe the jumps in both neurons due to synchronous input. The integral contains the contribution to $\rho(v_1, v_2, t)$ when a neuron pair with voltages $(V_1(t), V_2(t)) = (\theta_1, \theta_2)$ receives synchronous input of size $(v_1 - \theta_1, v_2 - \theta_2)$ that jumps the voltages to $(V_1(t), V_2(t)) = (v_1, v_2)$. The second term is due to loss of probability at $\rho(v_1, v_2, t)$ due to a neuron pair with voltages $(V_1(t), V_2(t)) = (v_1, v_2)$ receiving synchronous input that jumps both voltages higher.

The last three lines of Eq. (2) contain terms due to the reset of voltage to $V(t) = v_{\text{reset}}$ immediately after a neuron fires a spike. The factors $J_{\text{reset},k}$ are defined by

$$
\begin{aligned}
J_{\text{reset},1}(v_2, t) &= \nu_{\text{ind}}(t) \int_{v_{\text{reset}}}^{v_{\text{th}}} F_A(v_{\text{th}} - \theta_1)\rho(\theta_1, v_2, t)\mathrm{d}\theta_1 \\
&\quad + \nu_{\text{syn}}(t) \int_{v_{\text{reset}}}^{v_2} \int_{v_{\text{reset}}}^{v_{\text{th}}} F_A(v_{\text{th}} - \theta_1) f_A(v_2 - \theta_2) \\
&\quad \times \rho(\theta_1, \theta_2, t)\mathrm{d}\theta_1\mathrm{d}\theta_2, \\
J_{\text{reset},2}(v_1, t) &= \nu_{\text{ind}}(t) \int_{v_{\text{reset}}}^{v_{\text{th}}} F_A(v_{\text{th}} - \theta_2)\rho(v_1, \theta_2, t)\mathrm{d}\theta_2 \\
&\quad + \nu_{\text{syn}}(t) \int_{v_{\text{reset}}}^{v_{\text{th}}} \int_{v_{\text{reset}}}^{v_1} F_A(v_{\text{th}} - \theta_2) f_A(v_1 - \theta_1) \\
&\quad \times \rho(\theta_1, \theta_2, t)\mathrm{d}\theta_1\mathrm{d}\theta_2, \\
J_{\text{reset},3}(t) &= \nu_{\text{syn}}(t) \int_{v_{\text{reset}}}^{v_{\text{th}}} \int_{v_{\text{reset}}}^{v_{\text{th}}} F_A(v_{\text{th}} - \theta_1) \\
&\quad \times F_A(v_{\text{th}} - \theta_2)\rho(\theta_1, \theta_2, t)\mathrm{d}\theta_1\mathrm{d}\theta_2, \qquad (3)
\end{aligned}
$$

where $F_A(x)$ is the complementary cumulative distribution function of the random jump size A, that is, $F_A(x) = \int_x^\infty f_A(t)\mathrm{d}t = \Pr(A > x)$. The first integral of $J_{\text{reset},1}(v_2, t)$ reflects the event that a neuron with $V_1(t) = \theta_1$ receives an independent input that jumps the voltage past the threshold v_{th}. The neuron is reset to $V_1(t) = v_{\text{reset}}$ while $V_2(t)$ stays at v_2. The second integral of $J_{\text{reset},1}(v_2, t)$ reflects the event that a pair of neurons with $(V_1(t), V_2(t)) = (\theta_1, \theta_2)$ receives a simultaneous input that jumps $V_1(t)$ past threshold and $V_2(t)$ to the subthreshold voltage v_2. $J_{\text{reset},2}(v_1, t)$ is identical to $J_{\text{reset},1}(v_2, t)$ with the roles of the neurons reversed. $J_{\text{reset},3}(t)$ reflects the event that a pair of neurons with $(V_1(t), V_2(t)) = (\theta_1, \theta_2)$ receives a simultaneous input that jumps both neurons past threshold. In this case, both voltages are reset to v_{reset}. The neuron firings contributing to the $J_{\text{reset},k}$ are illustrated in Fig. 4.

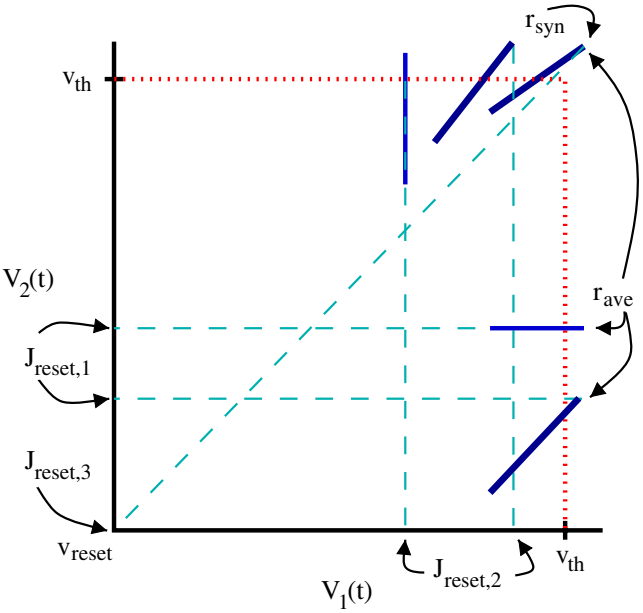

Fig. 4 Illustration of the three reset terms and their relationship to the average and synchronous firing rates. $J_{\text{reset},1}$ corresponds to the reset to v_{reset} after neuron 1 fires alone due to independent or synchronous input. $J_{\text{reset},2}$ is the equivalent for neuron 2. $J_{\text{reset},3}$ corresponds to the reset of both neurons to v_{reset} after synchronous input causes the neurons to simultaneously cross threshold. The synchronous firing rate r_{syn} is simply $J_{\text{reset},3}$. We can obtain the average firing rate r_{ave} by adding all the ways neuron 1 can fire alone (all the $J_{\text{reset},1}$) to the synchronous firing rate. Plotting convention is the same as in Fig. 3

The addition of the reset terms makes Eq. (2) a conservative system so that the integral of ρ remains constant, which we fix to 1. However, the equation is not written in conservative form. To aid in developing a conservative numerical method to solve Eq. (2), we first rewrite the equation in conservative form, and then base our numerical scheme on the conservative form, as discussed in Appendix A.

2.3 Total firing rate and synchronous firing rate

Since the reset terms described above reflect the voltage reset after firing, they can be used to read out

the firing rate of population. If we denote $V_j(T^+) = \lim_{t\to T^+} V_j(t)$, we can interpret the reset terms as

$$\begin{aligned} J_{\text{reset},1}(v_2,t)\mathrm{d}v_2\mathrm{d}t &= \Pr(\text{neuron 1 fires at } T\in(t,t+\mathrm{d}t) \\ &\qquad \text{and } V_2(T^+)\in(v_2,v_2+\mathrm{d}v_2)), \\ J_{\text{reset},2}(v_1,t)\mathrm{d}v_1\mathrm{d}t &= \Pr(\text{neuron 2 fires at } T\in(t,t+\mathrm{d}t) \\ &\qquad \text{and } V_1(T^+)\in(v_1,v_1+\mathrm{d}v_1)), \\ J_{\text{reset},3}(t)\mathrm{d}t &= \Pr(\text{both neurons simultaneously} \\ &\qquad \text{fire at } T\in(t,t+\mathrm{d}t)). \end{aligned} \tag{4}$$

Note that the factors $J_{\text{reset},1}(v_2,t)\mathrm{d}v_2$, $J_{\text{reset},2}(v_1,t)\mathrm{d}v_1$, and $J_{\text{reset},3}(t)$ indicate the probability of a spike per unit time. If neuron 1 fires a spike, the spike will be reflected in $J_{\text{reset},3}$ if neuron 2 fires simultaneously; otherwise the spike will be reflected in $J_{\text{reset},1}$. Therefore, the average firing rate for a neuron is simply the sum of $J_{\text{reset},3}(t)$ plus all of the $J_{\text{reset},1}(v_2,t)$,

$$r_{\text{ave}}(t) = \int_{v_{\text{reset}}}^{v_{\text{th}}} J_{\text{reset},1}(v_2,t)\mathrm{d}v_2 + J_{\text{reset},3}(t). \tag{5}$$

(By symmetry, we could have equally well defined $r_{\text{ave}}(t)$ by replacing $J_{\text{reset},1}$ with $J_{\text{reset},2}$, obtaining the identical firing rate of neuron 2).

We also define the synchronous firing rate, which is the rate at which both neurons fire simultaneously. Given Eq. (4), the synchronous firing rate is clearly

$$r_{\text{syn}}(t) = J_{\text{reset},3}(t). \tag{6}$$

Since the reset terms $J_{\text{reset},k}$ are calculated in the course of solving for $\rho(v_1,v_2,t)$, we can easily obtain the firing rates $r_{\text{ave}}(t)$ and $r_{\text{syn}}(t)$. The threshold crossings corresponding to the average and synchronous firing rates are illustrated in Fig. 4.

2.4 Capturing output correlation

The average firing rate $r_{\text{ave}}(t)$ captures the first order statistics of the population output, and the synchronous firing rate $r_{\text{syn}}(t)$ captures one type of second order statistic of the output, namely correlation with zero delay. However, $r_{\text{syn}}(t)$ does not capture all of the correlation between two neurons. If a pair of neurons receives independent Poisson input at rate $\nu_{\text{ind}}(t)$ and synchronous Poisson input at rate $\nu_{\text{syn}}(t)$, their spikes may become correlated at some non-zero delay, which is not captured by $r_{\text{syn}}(t)$.

Consider the snapshot of $\rho(v_1,v_2,t)$ in the left panel of Fig. 5. The synchronous input $\nu_{\text{syn}}(t)$ has increased the probability of the voltage combinations $(V_1(t), V_2(t))$ close to the diagonal, so that the positive correlation between $V_1(t)$ and $V_2(t)$ is clearly seen. For this reason, the probability for $(V_1(t), V_2(t))$ to be in the upper right corner (point A in middle panel of Fig. 5) is higher than it would be if the neurons were independent. If the neurons received a synchronous input while their voltages were near the upper right corner, they would be highly likely to simultaneously spike and reset (points B→C), contributing to the synchronous firing rate $r_{\text{syn}}(t)$. However, if the neurons each received independent input not exactly at the same time, then the neurons would be highly likely to fire with a short delay between their firing times (A→D→E→F in middle panel of Fig. 5). With a voltage distribution such as in left panel of Fig. 5, this independent input would still lead to correlations in the firing between the neurons because they would be more likely to fire within a short delay of each other than predicted by an independent distribution.

We cannot directly read out this delayed correlation from $\rho_2(v_1,v_2,t)$. If the voltage pair $(V_1(t), V_2(t))$ is near the upper right corner and the first neuron received an independent input, it would be highly likely to fire by itself, after which its voltage would be reset to v_{reset}. The voltage pair $(V_1(t), V_2(t))$ jumps to the upper left corner of $\rho_2(v_1,v_2,t)$ (point E in middle panel of Fig. 5), and the fact that the first neuron had just spiked is lost. Even if the second neuron receives an input shortly thereafter and fires a spike (point F), there is no way of determining the spike time of the first neuron from the fact that $(V_1(t), V_2(t))$ crosses the upper boundary of $\rho_2(v_1,v_2,t)$ somewhere near the upper left corner.

To read out the delayed correlation, we construct another density, which we call $\rho_{\text{cross}}(v_2,\tau;t_0)$, defined so that $\rho_{\text{cross}}(v_2,\tau;t_0)/r_{\text{ave}}(t_0)$ is the probability density of $V_2(t_0+\tau)$ conditioned on neuron 1 firing at time t_0 (right panel of Fig. 5). To compute the evolution of $\rho_{\text{cross}}(v_2,\tau;t_0)$ with respect to τ for a fixed t_0, we initialize it with the distribution of neuron 2 conditioned on neuron 1 spiking, i.e., $\rho_{\text{cross}}(v_2,0;t_0) = J_{\text{reset},1}(v_2,t_0) + \delta(v_2-v_{\text{reset}})J_{\text{reset},3}(t_0)$. (This corresponds to injecting points C and D in the right panel of Fig. 5.) Then, we evolve $\rho_{\text{cross}}(v_2,\tau;t_0)$ according a modified version of equation Eq. (2), where we integrated out v_1 and replaced t with $t_0+\tau$. We then define $r_{\text{cross}}(\tau;t_0)$ as the reset term from this modified equation (the D→E threshold crossing and subsequent reset in the right panel of Fig. 5). In this way, $r_{\text{cross}}(\tau;t_0)/r_{\text{ave}}(t_0)$ is the probability per unit time that neuron 2 fires at time $t_0+\tau$ conditioned on neuron 1 firing at time t_0. We subtract $r_{\text{ave}}(t_0+\tau)$, the marginal probability per unit time that neuron 2 fires at time $t_0+\tau$, and multiply by $r_{\text{ave}}(t_0)$. Finally, we add the zero delay correlation

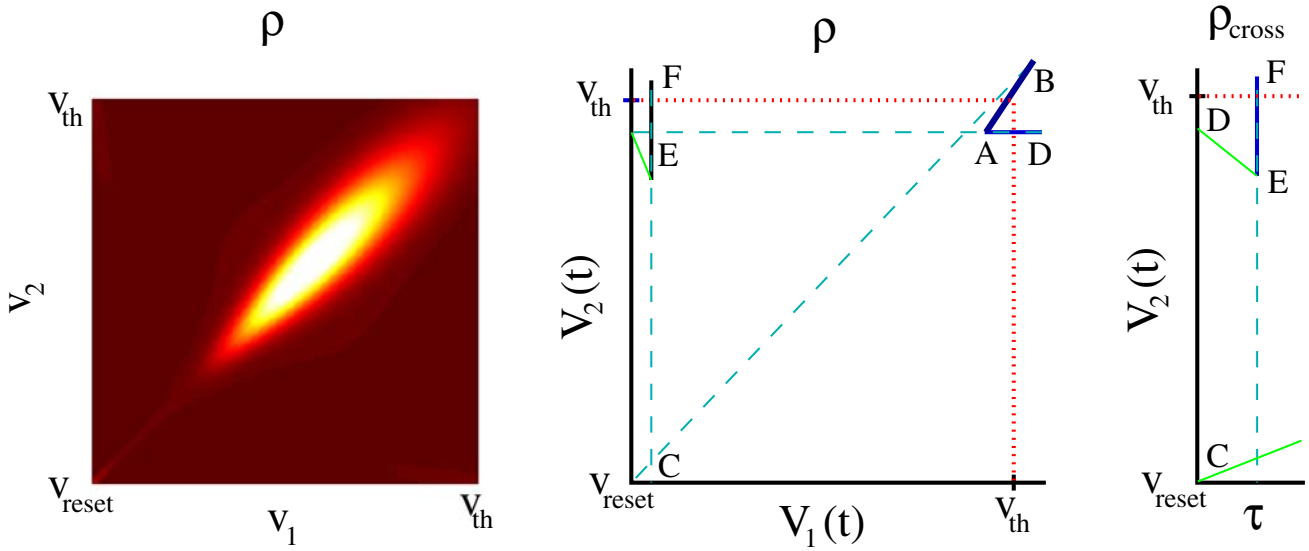

Fig. 5 *Left*: Pseudocolor plot of highly correlated population density function $\rho(v_1, v_2, t)$. Light colors correspond to high probability. *Middle*: Illustration of delayed correlation that is likely to result from a correlated population density. Given the correlated density, the likelihood that the voltages $(V_1(t), V_2(t))$ of a pair of neurons is in the *upper right corner* (A) is higher than if the voltages were independent. Receiving synchronous input might lead to synchronous firing and reset of the neuron pair (A→B→C). However, if the neurons each received independent input, the neurons would be likely to fire within a short delay (A→D→E→F). After the first neuron fires, the voltage is reset to the *upper left corner* (E), and the fact that the first neuron fired recently is lost. *Right*: Illustration of method to track delayed correlation. After the first neuron fires and the voltage pair is reset to (v_{reset}, v_2) in $\rho(v_1, v_2, t)$, the firing is simultaneously recorded by injecting into $\rho_{\text{cross}}(v_2, \tau; t)$ at $(v_2, 0)$ (point D on right diagram). As the voltage of the second neuron evolves (D→E), the time since the first neuron fired is tracked by τ. When the second neuron fires (E→F), the pair of spikes with delay τ (i.e., at times t and $t+\tau$) is recorded by the crossing of threshold in $\rho_{\text{cross}}(v_2, \tau; t)$ at the point (v_{th}, τ). If the neurons had fired simultaneously, we would record this by injecting into $\rho_{\text{cross}}(v_2, \tau; t)$ at $(v_{\text{reset}}, 0)$ (point C on *right diagram*). Plotting convention of the right two panels is the same as in Fig. 3

$r_{\text{syn}}(t_0)$ to obtain the cross correlation between the neurons at time t_0 with delay τ:

$$C(\tau; t_0) = \delta(\tau) r_{\text{syn}}(t_0) + r_{\text{cross}}(\tau; t_0) - r_{\text{ave}}(t_0) r_{\text{ave}}(t_0 + \tau). \quad (7)$$

The cross-correlation has units of spikes per unit time squared and is the correlation between spikes of one neuron at time t_0 and the spikes of a second neuron at time $t_0 + \tau$. We extend the definition for negative delays $-\tau$ to be the correlation between the spikes of one neuron at time $t_0 - \tau$ and the spikes of another neuron at time t_0: $C(-\tau; t_0) = C(\tau; t_0 - \tau)$. To summarize the correlation at a time t, we compute the area of the peak of positive correlation around delay 0,

$$C_{\text{peak}}(t) = \int_{-\tau_1}^{\tau_2} C(\tau; t) \mathrm{d}\tau, \quad (8)$$

where $-\tau_1$ and τ_2 are the delays where the correlation first becomes negative: $\tau_1 = \min\{\tau > 0 \,|\, C(-\tau, t) \le 0\}$ and $\tau_2 = \min\{\tau > 0 \,|\, C(\tau, t) \le 0\}$.

2.5 Derivation of network equations

The kinetic theory Eq. (2) can be used to compute the evolution of a population of neurons to prescribed independent and synchronous input rates, $\nu_{\text{ind}}(t)$ and $\nu_{\text{syn}}(t)$ respectively. Along with the evolution of the population density $\rho(v_1, v_2, t)$, we also compute the output statistics: the average firing rate $r_{\text{ave}}(t)$, the synchronous firing rate $r_{\text{syn}}(t)$, and the output correlation $C(\tau; t)$. To apply our results to a feed-forward network, we need a method to transform the output of a presynaptic population to the input of a postsynaptic population, taking into account the statistics of the connectivity.

As mentioned in Section 1.2, we will characterize the connectivity between two populations by both first and second order statistics. The first order statistic is W^1_{jk}, the expected number of presynaptic neurons from population j that project to any postsynaptic neuron in population k. The second order statistics is W^2_{jk}, the expected number of presynaptic neurons from population j that simultaneously project to any pair of postsynaptic neurons in population k. Our goal is to compute the input rates $\nu^k_{\text{ind}}(t)$ and $\nu^k_{\text{syn}}(t)$ to population

k based on these connectivity statistics, the output of each population j, and any external independent input to population k at rate $\nu^k_{\text{ext}}(t)$. We assume that neurons from different populations are uncorrelated and neurons within a population are uncoupled.

We consider a pair of neurons in population k. Let N_1^j be the number of neurons from population j that project onto the first neuron and N_2^j be the number of neurons that project onto the second neuron. Furthermore, let N_3^j be the number of neurons from population j that project onto both postsynaptic neurons. (In the illustration of Fig. 2, $N_1^j = 5$, $N_2^j = 7$ and $N_3^j = 2$). We view N_1^j, N_2^j, and N_3^j as three random numbers with expected values specified by the connectivity statistics: $E\left(N_1^j\right) = E\left(N_2^j\right) = W^1_{jk}$ and $E\left(N_3^j\right) = W^2_{jk}$. To calculate the input rates $\nu^k_{\text{ind}}(t)$ and $\nu^k_{\text{syn}}(t)$, we will first calculate them conditioned on particular values of $\mathbf{N}_{\text{in}} = \left\{N_i^j\right\}$ and then take the expected values over the $\mathbf{N}_{\text{in}}$.

Define $\nu^k_{\text{syn}}(t; \mathbf{N}_{\text{in}})$ to be the rate of synchronous input onto neurons 1 and 2, conditioned on particular values of the $\mathbf{N}_{\text{in}}$. We calculate that this input rate is

$$\begin{aligned}\nu^k_{\text{syn}}(t; \mathbf{N}_{\text{in}}) &= \sum_j N_3^j \left(r^j_{\text{ave}}(t) - r^j_{\text{syn}}(t)\right) \\ &\quad + \sum_j \Big[\left(N_1^j - N_3^j\right)\left(N_2^j - N_3^j\right) + \left(N_1^j - N_3^j\right) N_3^j \\ &\quad + \left(N_2^j - N_3^j\right) N_3^j + 2\binom{N_3^j}{2}\Big] r^j_{\text{syn}}(t) \\ &= \sum_j \left[N_3^j r^j_{\text{ave}}(t) + \left(N_1^j N_2^j - 2N_3^j\right) r^j_{\text{syn}}(t)\right]. \quad (9)\end{aligned}$$

The neurons will receive synchronous input any time one of the N_3^j neuron projecting to both neurons fires a spike all by itself (i.e., no other of the presynaptic neurons fires synchronously with it). Since we are calculating only up to second order statistics, we can approximate the probability per unit time that just a single neuron fires as $r^j_{\text{ave}}(t) - r^j_{\text{syn}}(t)$. Multiplying by the number N_3^j of common input neurons, we obtain the first sum of Eq. (9).

The second sum of Eq. (9) accounts for the synchronous input to neurons 1 and 2 that results from one of the N_1^j neurons projecting to neuron 1 firing synchronously with one of the N_2^j neurons projecting to neuron 2. This could happen in four ways, corresponding to the four terms in the square brackets. First, one of the $\left(N_1^j - N_3^j\right)$ neurons projecting to neuron 1 alone could fire synchronously with one of the $\left(N_2^j - N_3^j\right)$ neurons projecting to neuron 2 alone. Second, one of the $\left(N_1^j - N_3^j\right)$ neurons projecting to neuron 1 alone could fire synchronous with one of the N_3^j common input neurons. In this case, neuron 1 receives a double input that is synchronous to a single input to neuron 2. Since our kinetic theory description does not represent double inputs to any neuron, we represent this event just as synchronous input to the pair. Third, we handle in the same way the event where one of the N_3^j common input neuron fires synchronously with one of the $\left(N_2^j - N_3^j\right)$ neurons projecting to neuron 2 alone. Fourth, if two of the N_3^j common input neurons fire synchronously, both neurons 1 and 2 receive synchronous double inputs. Since our kinetic theory does not represent double inputs, we model the double synchronous inputs as two synchronous inputs. Hence, we multiply the number of pairs $\binom{N_3^j}{2}$ by two. All these combinations of inputs are multiplied by the probability per unit time $r^j_{\text{syn}}(t)$ that two input neurons fire synchronously.

The approximations used for the last three terms in the second sum of Eq. (9) can be justified under the condition that $N_3^j \ll N_1^j$ and $r_{\text{syn}} \ll r_{\text{ave}}$. If common input neurons are relatively rare and the synchrony isn't too high, then these last three terms will be small (quadratic in a small parameter) compared to the other terms of Eq. (9). For this reason, we expect our kinetic theory implementation to perform best under conditions where the synchronous firing and fraction of shared input are not too high.

Next, we take the expected value of $\nu^k_{\text{syn}}(t; \mathbf{N}_{\text{in}})$ over $\mathbf{N}_{\text{in}}$. The only expected value not explicitly specified by our second order connectivity statistics is the product $E\left(N_1^j N_2^j\right)$. We simply assume that N_1^j and N_2^j are uncorrelated so that $E\left(N_1^j N_2^j\right) = E\left(N_1^j\right) E\left(N_2^j\right)$. We obtain that the expected rate of synchronous input is

$$\begin{aligned}\nu^k_{\text{syn}}(t) &= E\left(\nu^k_{\text{syn}}(t; \mathbf{N}_{\text{in}})\right) \\ &= \sum_j W^2_{jk} r^j_{\text{ave}}(t) + \sum_j \left(W^1_{jk} W^1_{jk} - 2W^2_{jk}\right) r^j_{\text{syn}}(t) \\ &= \sum_j \beta_{jk} W^1_{jk} r^j_{\text{ave}}(t) + \sum_j W^1_{jk}\left(W^1_{jk} - 2\beta_{jk}\right) r^j_{\text{syn}}(t), \\ &\quad (10)\end{aligned}$$

where $\beta_{jk} = W^2_{jk}/W^1_{jk}$ is the fraction of shared input parameter.

The average input to population k is simply the external input rate $\nu^k_{\text{ext}}(t)$ plus the sum of the $W^1_{jk} r^j_{\text{ave}}(t)$, the average coupling times the average firing rate. As discussed in Section 2.4, the output of population j will

contain correlations beyond the synchronous output of $r^j_{\text{syn}}(t)$. However, our kinetic theory equations do not include delayed correlation in the input. (We neglected delayed correlation to create a Markov process without adding additional state variables.) For our first approximation, which we term *KT0*, we will simply assume that inputs that are not synchronous are independent. Under this approximation, the independent input rate to population k is simply the average input rate minus the synchronous input rate:

$$\nu^k_{\text{ind}}(t) = \nu^k_{\text{ext}}(t) + \sum_j W^1_{jk} r^j_{\text{ave}}(t) - \nu^k_{\text{syn}}(t). \tag{11}$$

This formula not only neglects delayed correlation, but it also approximates as independent any double input to a single neuron. (Such double inputs would occur when a pair of neurons projecting to the given neuron fire synchronously).

2.6 Accounting for delayed correlation

The delayed correlation described in Section 2.4 may be more substantial than the instantaneous correlation reflected in $r_{\text{syn}}(t)$. In this case, we may severely underestimate the correlation by assuming all spikes not captured by $r_{\text{syn}}(t)$ are independent, as we did for deriving the coupling conditions (10) and (11). Hence, we developed another method to capture additional correlation in our kinetic theory implementation. We approximated delayed correlation in the output of a population as though it were correlation with zero delay.

Approximating delayed correlation as instantaneous is not as simple as adding $C_{\text{peak}}(t)$ of Eq. (8) to $r_{\text{syn}}(t)$. The cross-correlation peak area $C_{\text{peak}}(t)$ evaluated at time t is based on output from times $t+\tau$ that are later than t. If we included $C_{\text{peak}}(t)$ in the input rates at time t, we would be attempting to use future information to calculate the evolution of the network at time t.

To avoid using future information, we calculate a modified version of the cross-correlation (7) based on a quasi-steady state approximation. Rather than using the density $\rho_{\text{cross}}(v_2, \tau; t_0)$ introduced in Section 2.4, we calculate the evolution of another density-like quantity that we call $\rho_{\text{delay}}(v_2, \tau; t_0)$. We calculate the evolution of ρ_{delay} in the same way as ρ_{cross} except that we freeze the input rates at $\nu_{\text{ind}}(t_0)$ and $\nu_{\text{syn}}(t_0)$. Moreover, in ρ_{delay}, we wish to look only at the first spike of neuron 2 after the spike of neuron 1. For this reason, we do not include the reset terms when evolving ρ_{delay}. To subtract off the expected distribution of v_2 under the assumption that the neurons were independent, we initialize ρ_{delay} by subtracting off the marginal distribution of ρ, multiplied by the average firing rate: $\rho_{\text{delay}}(v_2, 0; t_0) = J_{\text{reset},1}(v_2, t_0) - r_{\text{ave}}(t_0) \int \rho(v_1, v_2, t_0) \mathrm{d}v_1$. Although we do not reinject the reset term into the evolution equation for ρ_{delay}, we still define $c_{\text{delay}}(\tau, t_0)$ as the magnitude of this reset term (or, equivalently, the flux across threshold). Since we subtracted off the marginal density in defining $\rho_{\text{delay}}(v_2, 0; t_0)$, the reset quantity $c_{\text{delay}}(\tau, t_0)$ reflects how much more likely neuron 2 was to fire than it would have fired if the neurons were independent. In other words, $c_{\text{delay}}(\tau, t)$ represents the delayed correlation between the spikes of one neuron at time t and the subsequent spike of another neuron, subject to the quasi-steady state approximation that uses no future information beyond the time t. Given the quasi-steady state approximation, the correlation with negative delay is symmetric to the correlation with positive delay, and we define $c_{\text{delay}}(-\tau, t) = c_{\text{delay}}(\tau, t)$ for $\tau > 0$. The resulting correlation magnitude analogous to $C_{\text{peak}}(t)$ is

$$\tilde{r}_{\text{syn}}(t) = r_{\text{syn}}(t) + \int_{-\tau_0}^{\tau_0} c_{\text{delay}}(\tau, t) \mathrm{d}\tau \tag{12}$$

where τ_0 is the delay where $c_{\text{delay}}(\tau, t)$ first becomes negative: $\tau_0 = \min\{\tau > 0 \,|\, c_{\text{delay}}(\tau, t) \le 0\}$. We denote this correlation by $\tilde{r}_{\text{syn}}(t)$ because we will use $\tilde{r}_{\text{syn}}(t)$ in place of the synchronous firing rate $r_{\text{syn}}(t)$ in the coupling Eqs. (10) and (11), effectively assuming that this correlation was due to synchronous spiking of the presynaptic neurons. Since we have not included reset in the calculation of c_{delay}, we know that the condition $\tilde{r}_{\text{syn}}(t) \le r_{\text{ave}}(t)$ is always satisfied.

Our new connectivity equations (reintroducing superscripts to denote population index) are

$$\nu^k_{\text{syn}}(t) = \sum_j \beta_{jk} W^1_{jk} r^j_{\text{ave}}(t) + \sum_j W^1_{jk} \left(W^1_{jk} - 2\beta_{jk} \right) \tilde{r}^j_{\text{syn}}(t) \tag{13}$$

$$\nu^k_{\text{ind}}(t) = \nu^k_{\text{ext}}(t) + \sum_j W^1_{jk} r^j_{\text{ave}}(t) - \nu^k_{\text{syn}}(t). \tag{14}$$

We refer to this improved kinetic theory implementation that accounts for delayed correlations as *KT1*.

Note that there is no guarantee that $\nu^k_{\text{ind}}(t)$ defined by the above equation will be positive, despite the fact that we know $\tilde{r}^j_{\text{syn}}(t) \le r^j_{\text{ave}}(t)$. It is possible for the synchronous input $\nu^k_{\text{syn}}(t)$ calculated from Eq. (13) to

exceed the total input from presynaptic populations $\sum_j W^1_{jk} r^j_{\text{ave}}(t)$. Such a nonphysical result is due to neglecting the possibility of three or more simultaneous inputs. As detailed in Section 4, such combinations become highly likely as the correlation increases. To keep physically meaningful values of $\nu^k_{\text{syn}}(t)$, we simply truncate it to $\sum_j W^1_{jk} r^j_{\text{ave}}(t)$, the total input from presynaptic populations, if the quantity calculated from Eq. (13) or Eq. (10) exceeds that sum.

The Eqs. (13) or (10) for $\nu_{\text{syn}}(t)$ contain two sources for the correlated input to a population. The first sum describes the emergence of correlations due to the shared input between a pair of neurons. For example, when either of the common input neurons of Fig. 2 spikes, it will send synchronous input into the pair of postsynaptic neurons. The second sum describes the propagation of correlations through the network. For example, when a light and dark presynaptic neuron of Fig. 2 spike synchronously, they send synchronous input to the postsynaptic neuron pair even though no connections are shared. The subtraction of 2β is an approximate correction to control for overcounting when a common input neuron fires synchronously with another input neuron. In this way, the kinetic theory network is designed to capture the emergence and propagation of correlations in the network and describe the second order statistics of the network activity.

3 Results

We demonstrate our kinetic theory approach by benchmarking its output against Monte Carlo simulations of networks of integrate-and-fire neurons. We first compare simulations of a single population of non-interacting neurons in order to demonstrate that the kinetic theory does accurately represent the response of neurons to correlated input. Second, we compare simulations of feed-forward networks in order to investigate how well our kinetic theory implementation captures the emergence and propagation of correlations through a network. We simulated the Monte-Carlo networks as described in Nykamp and Tranchina (2000).

3.1 Single population

As an initial test of our kinetic theory approach, we simulated the response of a single population of neurons to correlated input. We numerically solved the kinetic theory equations (2) as described in Appendix A in response to specified independent $\nu_{\text{ind}}(t)$ and synchronous $\nu_{\text{syn}}(t)$ input rates. Since these single population runs did not include any network interactions, they simply reflect the ability of the kinetic theory to capture the correlated output of neurons in response to correlated input.

To test the accuracy of the kinetic theory solution, we simulated 500,000 realizations of a pair of integrate-and-fire neurons in response to the same input rates. We stimulated each neuron with an independent Poisson process with rate $\nu_{\text{ind}}(t)$. We also stimulated both neurons with a third Poisson process with rate $\nu_{\text{syn}}(t)$. Since the input to the neurons was Poisson and correlated only with zero delay, these Monte Carlo simulations exactly matched the assumptions of our kinetic theory model. In this way, the Monte Carlo simulations served simply to test if we correctly implemented our kinetic theory equations.

Results of one such test are shown in Fig. 6. For this example, we set the independent input rate $\nu_{\text{ind}}(t)$ to 150 spikes per second and the synchronous input rate $\nu_{\text{syn}}(t)$ to 100 spikes per second, and allowed the population to achieve steady state. Then, we kept the same input rates until $t = 0.05$ s, at which point we doubled the input rates to $\nu_{\text{ind}}(t) = 300$ and $\nu_{\text{syn}}(t) = 200$ spikes per second. In response, the average firing rate $r_{\text{ave}}(t)$, the synchronous firing rate $r_{\text{syn}}(t)$, and the cross-correlation peak area $C_{\text{peak}}(t)$ immediately jumped to higher values and then settled down to new steady state values. As expected, the kinetic theory and Monte Carlo estimates matched exactly in all three cases (Fig. 6(a)). Note that $C_{\text{peak}}(t)$ began to increase even before the time of the input change due to the fact that it includes correlation of spikes at time t with spikes at future times.

The kinetic theory also accurately captures the form of the delayed correlation resulting from the correlated input. As shown in Fig. 6(b), the structure of the cross-correlation averaged over all neuron pairs is precisely matched by the kinetic theory. Note that for each pair (j, k) of neurons, the correlation at a delay τ includes the effect of neuron j spiking after neuron k and neuron k spiking after neuron j. Therefore, since there is no structure in the input at steady state, the cross-correlation must be symmetric with respect to delay (Fig. 6(b), top). The asymmetry in the transient cross-correlation (Fig. 6(b), bottom) is due to the asymmetric population activity around the sampled time point. We obtained equally good matches between kinetic theory and Monte Carlo simulations for every other input rate ($\nu_{\text{ind}}(t)$ and $\nu_{\text{syn}}(t)$) combination we tested. These results are not surprising because the input in the Monte Carlo simulations was chosen to exactly match the assumptions of our kinetic theory implementation. The results simply serve as verification that we are solving our kinetic theory equations correctly.

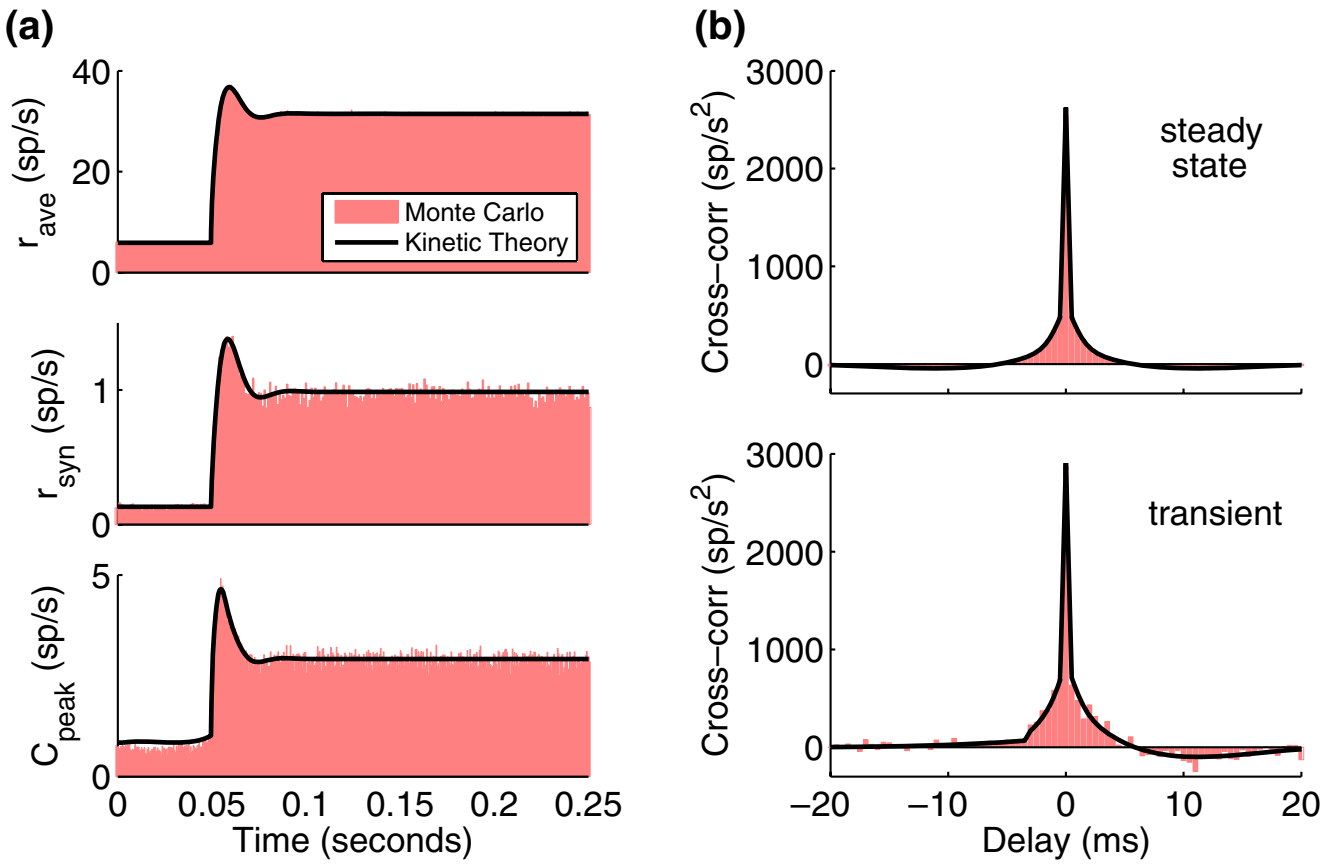

Fig. 6 Results from a single population of uncoupled neurons. The kinetic theory results exactly match those from Monte Carlo simulations. (**a**) Average firing $r_{\text{ave}}(t)$ (top), synchronous firing rate $r_{\text{syn}}(t)$ (*middle*), and cross-correlation peak area $C_{\text{peak}}(t)$ (*bottom*) are plotted in response to a jump in independent $\nu_{\text{ind}}(t)$ and synchronous $\nu_{\text{syn}}(t)$ input rate at time $t = 0.05$ s. The histograms from the Monte Carlo simulations coincide with the values obtained from solving the kinetic theory equations. (**b**) Cross-correlation averaged over the steady state ($t > 0.15$ s) and cross-correlation from the transient peak in $C_{\text{peak}}(t)$ ($t = 0.054$ s) are plotted versus delay. The Monte-Carlo data was binned using a bin width of $\Delta t = 0.5$ ms. The kinetic theory cross-correlation contains a delta function at zero delay. The delta-function magnitude was divided by $\Delta t = 0.0005$ s and added to the value of the continuous correlation at zero delay. Since the kinetic theory correlation is sampled every half millisecond, this procedure effectively smooths the delta-function over a half millisecond window so that the results match the bin width used in Monte Carlo

3.2 Feed-forward network

To test the ability of our kinetic theory implementation to capture the emergence and propagation of correlations through a network, we examined its performance with a ten layer feed-forward network. It is well-known that synchronous activity develops in deeper layers of a feed-forward network (Diesmann et al. 1999; Câteau and Fukai 2001; Reyes 2003; Hasegawa 2003; Wang et al. 2006; Masuda and Aihara 2002; Litvak et al. 2003; van Rossum et al. 2002; Doiron et al. 2006). By comparing the kinetic theory results to Monte Carlo simulations of the feed-forward network, we could assess how well the kinetic theory could model the build-up of correlations underlying such synchrony.

3.2.1 Illustration of the build-up of correlations

To illustrate the build-up of correlations, we simulated the response of feed-forward networks to a step input, where at time t_0 we instantaneously increased the independent Poisson input to layer 1 from $\nu^1_{\text{ind,ext}}(t) = 200$ spikes per second to $\nu^1_{\text{ind,ext}}(t) = 300$. Each layer $k > 1$ received independent Poisson input at constant rate $\nu^k_{\text{ind,ext}}(t) = 200$ in addition to the input from the previous layer. Unlike the single population simulations, we did not add any external synchronous input as we wished to explore the synchrony that emerged from the network.

We created networks with N neurons per layer and randomly connected neurons from each layer onto the

subsequent layer so that the expected number of connections onto each neuron was $W^1 = 10$. (To accomplish this, we randomly selected each of the possible N^2 connections between a pair of layers with probability W^1/N).

An example of the emergent synchronous activity in feed-forward networks is illustrated in Fig. 7(a). For the network with $N = 100$ neurons per layer (Fig. 7(a), left column), peaks in the histogram begin to emerge in layer 6 and become prominent in layer 10. These peaks correspond to many neurons firing synchronously within a $\Delta t = 10$ ms time window, as the histogram is based on a bin width of Δt.

In the network with $N = 1{,}000$ neurons per layer (Fig. 7(a), right column), this synchrony does not appear to emerge, at least in 10 layers, as the histograms remain relatively flat even in layer 10. Such observations make it seem that such synchronization is a finite-size effect and that the number of neurons N plays a critical role in determining the emergence of synchrony (Doiron et al. 2006). We will reexamine this hypothesis below.

The build-up of correlations is illustrated in Fig. 7(b). For the network with $N = 100$ neurons per layer (Fig. 7(b), left column), the cross-correlation for layer 6 contains a large peak centered around zero delay, and this peak is much larger in layer 10. On the other hand, when $N = 1{,}000$, the cross-correlation has only a small peak even in layer 10 (Fig. 7(b), right column). Our goal is to capture this build-up of correlation with our kinetic theory model.

The difficulty of capturing the synchrony with kinetic theory models is illustrated in Fig. 8. The kinetic theory can be thought of as representing the distribution of neuron responses over many realizations of the network response. Figure 8 shows histograms of the spikes of layer 10 of the network with $N = 100$ neurons per layer. For each of the four top panels, the same input used for Fig. 7(a) was presented, except that the step in input rate to layer 1 (i.e. the stimulus) occurred at

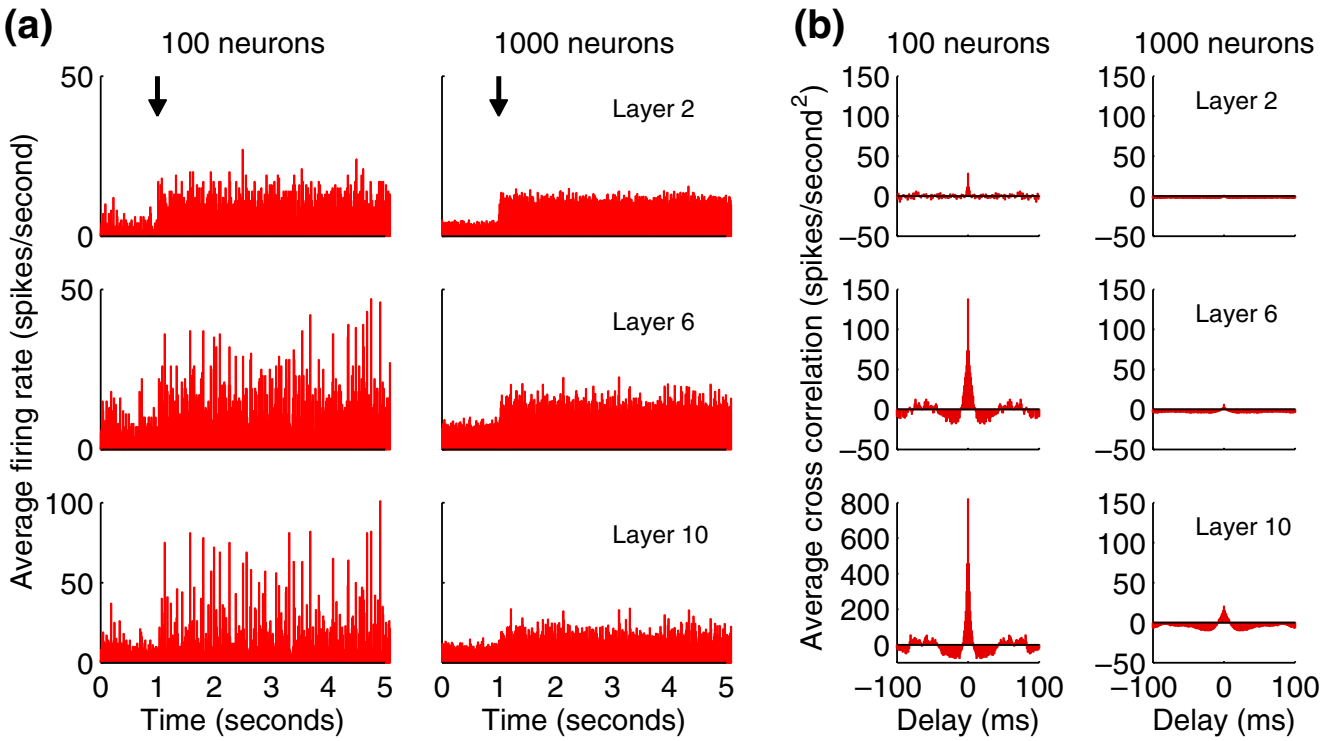

Fig. 7 Illustration of the build-up of correlations within a feed-forward network with ten layers. (**a**) A histogram of the firing times of all neurons in a layer binned at $\Delta t = 10$ ms, normalized to firing rate in spikes per second. The input rate to layer 1 was increased at time $t_0 = 1$ s (indicated by the *arrow*). Layers 2, 6, and 10 are shown for a network with $N = 100$ neurons per layer (*left column*) and $N = 1{,}000$ neurons per layer (*right column*). For the $N = 100$ network, sharp peaks in the histograms of layers 6 and 10 indicate simultaneous firing of many neurons within a single time bin. For the $N = 1{,}000$ network, although the neurons are firing at a similar rate, no strong peaks indicating synchrony are visible. (**b**) The cross-correlation calculated from the steady state ($t > 2$ s) and averaged among all pairs of neurons. Each panel corresponds to the simulation of the respective panel in (**a**). For the network with $N = 100$ neurons per layer, a strong peak in the cross-correlation is evident in layers 6 and 10 (note different scale for layer 10). For the $N = 1{,}000$ network, the correlation is small even in layer 10

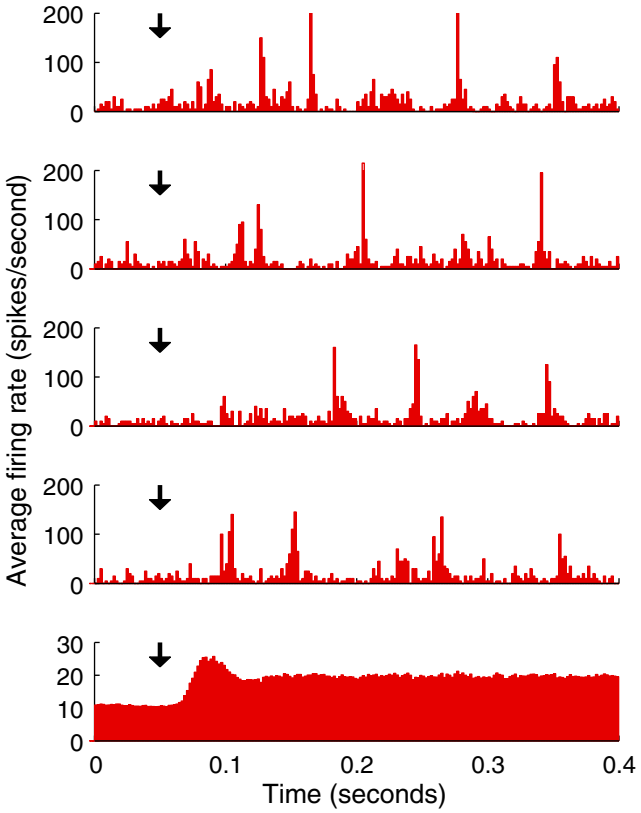

Fig. 8 The timing of synchronous bursts of activity will vary with different presentations of the same input. The feed-forward network with $N = 100$ neurons per layer was repeatedly stimulated with the input of Fig. 7, except that the step of the input occurred at $t_0 = 0.05$ s (*arrows*). The histogram of activity of the layer 10 neurons in response to four different presentations is shown in the top four panels. Plot is the same as the bottom left of Fig. 7 except for a smaller bin width of $\Delta t = 2$ ms and smaller range of times. The *bottom panel* is a peristimulus time histogram (PSTH) showing the average of 4,000 such presentations of the stimulus. Since the synchronous peaks in response to different presentations occurred at different times, the PSTH averages out the peaks and is flat after an initial transient

$t_0 = 0.05$ s. In this case, we bin the spikes at a smaller resolution of $\Delta t = 2$ ms and show only 0.4 s of data. In response to each of the four stimulus presentations, the layer 10 neurons show a high degree of synchrony as evidenced by the sharp peaks in the histograms. However, as the stimulus after t_0 is constant, there is no temporal structure that could align the times at which those peaks occur. Hence, in each of the four presentations, the synchronous peaks occur at different times.

The average over 4,000 stimulus presentations is shown in the bottom panel of Fig. 8. In this peristimulus time histogram (PSTH) we see a transient of increased firing rate soon after t_0, but then the firing rate settles down to a constant value. There is no indication that the neurons actually continued to fire synchronously. Due to the distribution of different times of the synchronous peaks, the average removes all of the temporal structure in the firing rate.

Since kinetic theory represents this average response, the average firing rate $r_{\text{ave}}(t)$ will not include any evidence of the synchronous firing, but instead should approach a constant value during the steady state period. We cannot capture the synchronous peaks of Fig. 7(a). Instead, our goal is a kinetic theory representation of the feed-forward network that captures the build-up of correlations of Fig. 7(b).

3.2.2 Demonstration of kinetic theory results

To compare the kinetic theory with the Monte Carlo simulations of the feed-forward networks, the first step is to calculate the connectivity statistics for the kinetic theory discussed in Section 2.5. As described above, we generate connections between two layers so that each connection has probability W^1/N, where N is the number of neurons per layer and $W^1 = 10$. Since for a given postsynaptic neuron, N possible connections are chosen with probability W^1/N, the number W^1 is the expected number of connections.

The expected number of shared connections onto any pair of postsynaptic neurons can be calculated from the assumption that all connections are generated independently. For any of the N possible presynaptic neurons, it has probability W^1/N being connected to the first neuron of the pair and probability W^1/N being connected to the second. Given that the connections are generated independently, the probability of being connection to both neurons in the pair is simply $(W^1/N)^2$. Multiplying by the N possible presynaptic neurons, and we calculate that the expected number of shared connections onto any pair of neurons is $W^2 = (W^1)^2/N$. Hence, the fraction of shared connections parameter is $\beta = W^2/W^1 = W^1/N$.

We simulated feed-forward networks with $N = 50$, 100, 200, and 1,000 neurons per population. We randomly generated a single network and presented the above step input $400{,}000/N$ times, as in Fig. 8. Before beginning each presentation, we allowed the network to equilibrate to steady state in response to the lower input rate ($\nu^k_{\text{ind}}(t) = 200$ spikes per second for all layers). Then, we began to record spikes and jumped the input to layer 1 up to $\nu^1_{\text{ind}}(t) = 300$ spikes per second at time $t_0 = 0.05$ s.

For each N, we calculated $\beta = W^1/N$ and created a kinetic theory representation of the network. The kinetic theory network consisted of ten population, where each population corresponded to a layer of the

network. We initially numerically solved the kinetic theory equations in response to the lower input rate ($\nu^k_{\text{ind}}(t) = 200$ spikes per second for all layers) to calculate the steady state distribution for that input. Using that distribution as the initial conditions, we numerically solved the kinetic theory equations in response to the input described above, increasing the input to layer one at time $t_0 = 0.05$ s.

For each network, we computed the kinetic theory response using two methods of approximating delayed correlation in the output of each population. In the first method (KT0), we ignored any correlation with non-zero delay in the output of each presynaptic population and computed the input to the corresponding postsynaptic population as though non-synchronous spikes were independent (using Eqs. (10) and (11) to connect populations). In the second method (KT1), we approximated delayed correlation as though it were correlation with zero delay (using Eqs. (13) and (14) to connect populations). In either case, the input to each population $k > 1$ was a combination of independent and synchronous Poisson input; we did not include delayed input correlation in our kinetic theory implementation.

The results for $\beta = 0.05$ (i.e., $N = 200$ in the Monte Carlo simulations) are shown in Fig. 9. The average firing rate $r_{\text{ave}}(t)$ (Fig. 9(a)) of the kinetic theory closely matched the Monte Carlo for both KT0 and KT1. At least for this network, assuming Poisson input to each layer did not greatly alter the first order output statistic $r_{\text{ave}}(t)$.

For the cross-correlation peak area $C_{\text{peak}}(t)$ (Fig. 9(b)), the results had a dramatic dependence

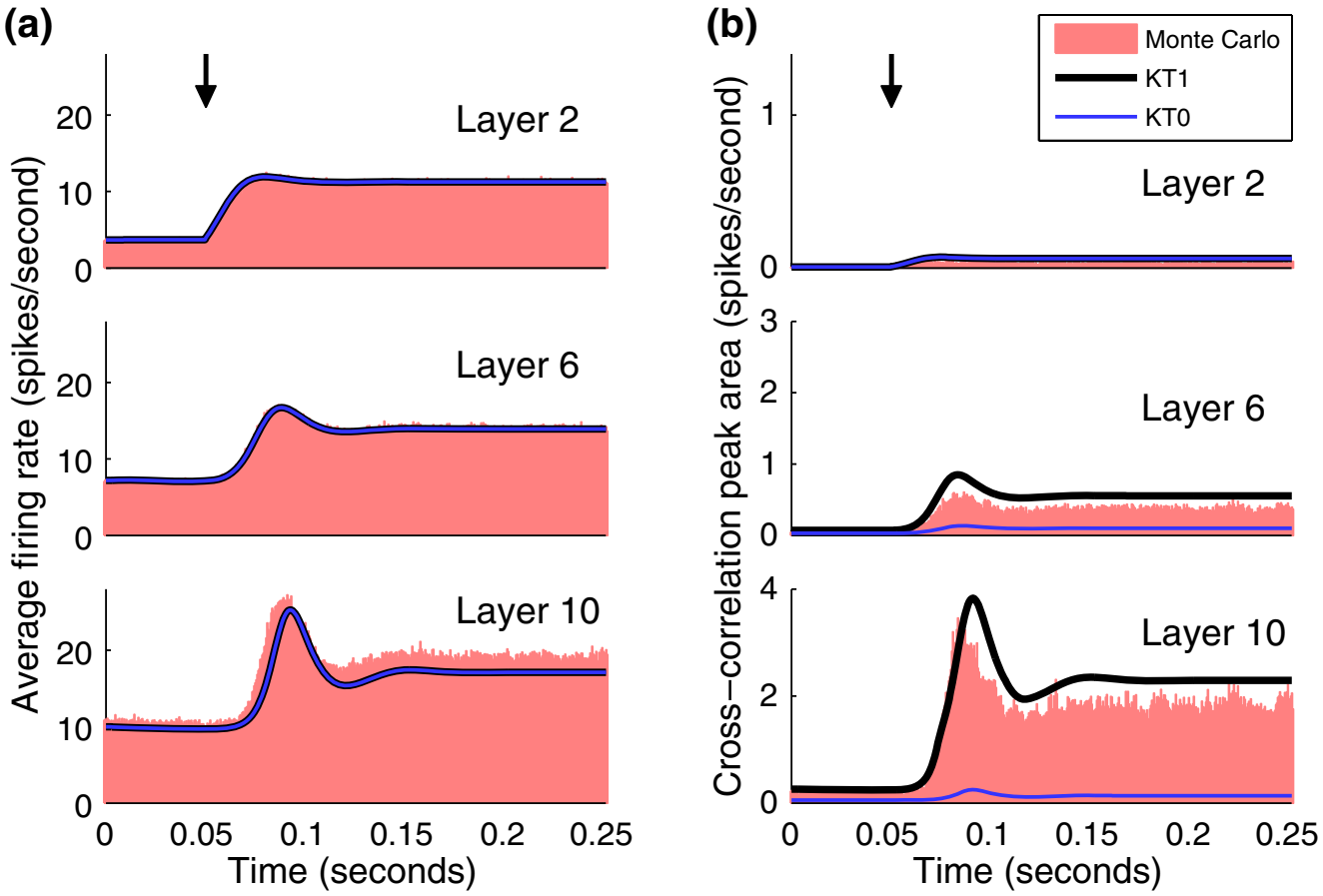

Fig. 9 Comparison of Monte Carlo and kinetic theory results for the network with $\beta = 0.05$ ($N = 200$ in Monte Carlo). The input rate to layer 1 is stepped up at time $t_0 = 0.05$ s (*arrows*). (**a**) The average firing rate $r_{\text{ave}}(t)$ is plotted for layers 2, 6, and 10. For Monte Carlo simulations, we plot a normalized peristimulus time histogram. The kinetic theory results based on ignoring delayed correlation in the neural output (KT0) are plotted by the *thin line*. The *thick line* indicates the kinetic theory results where delayed correlation is approximated as though it were instantaneous correlation (KT1). Both kinetic theory approximations result in nearly identical estimates of $r_{\text{ave}}(t)$, which underestimate the Monte Carlo results only slightly in the deeper layers. (**b**) The cross-correlation peak area $C_{\text{peak}}(t)$ is plotted for layers 2, 6 and 10. The same plotting convention as panel (**a**) is followed. KT0 fails to show the build-up of correlation in deeper layers. KT1 captures the correlation build-up, though correlation magnitude is overestimated

on the delayed correlation method. If we completely ignored delayed correlation (KT0), the kinetic theory failed to show the build-up in the correlation in the deeper layers of the network. On the other hand, when we approximated delayed correlation as instantaneous correlation (KT1), the kinetic theory was able to show the correlation increase. As instantaneous correlation has a stronger effect on neural response than delayed correlation, the approximation resulted in an overestimation of the actual magnitude of the correlation peak. But, the method captured the essence of how the correlations built up in the network.

Clearly, completely ignoring delayed correlation (KT0) fails miserably to capture the build-up of correlations. Approximating delayed correlation as instantaneous correlation (KT1) appears to be a much better method to handle the delayed correlation. From now on, we will focus our attention on KT1.

If we doubled the fraction of shared input to $\beta = 0.1$ (halved the number of neurons to the $N = 100$ of Figs. 7 and 8), our kinetic theory implementation matched the Monte Carlo results less accurately (Fig. 10). KT1 captures the build-up of correlations up through layer 6, still overestimating the correlation magnitude. However, by layer 10, correlation peak area calculated by KT1 is only about 70% that of the Monte Carlo at steady state. Even the first order statistic $r_{\text{ave}}(t)$ is slightly underestimated by KT1. The approximations underlying our kinetic theory implementation do indeed begin to break down at this high level of correlation, as predicted by the assumptions of our derivation in Section 2.5. We discuss some practical remedies in Section 4.

We examine the structure of the steady-state cross-correlation for these two networks in Fig. 11. Since we approximated delayed correlation as instantaneous,

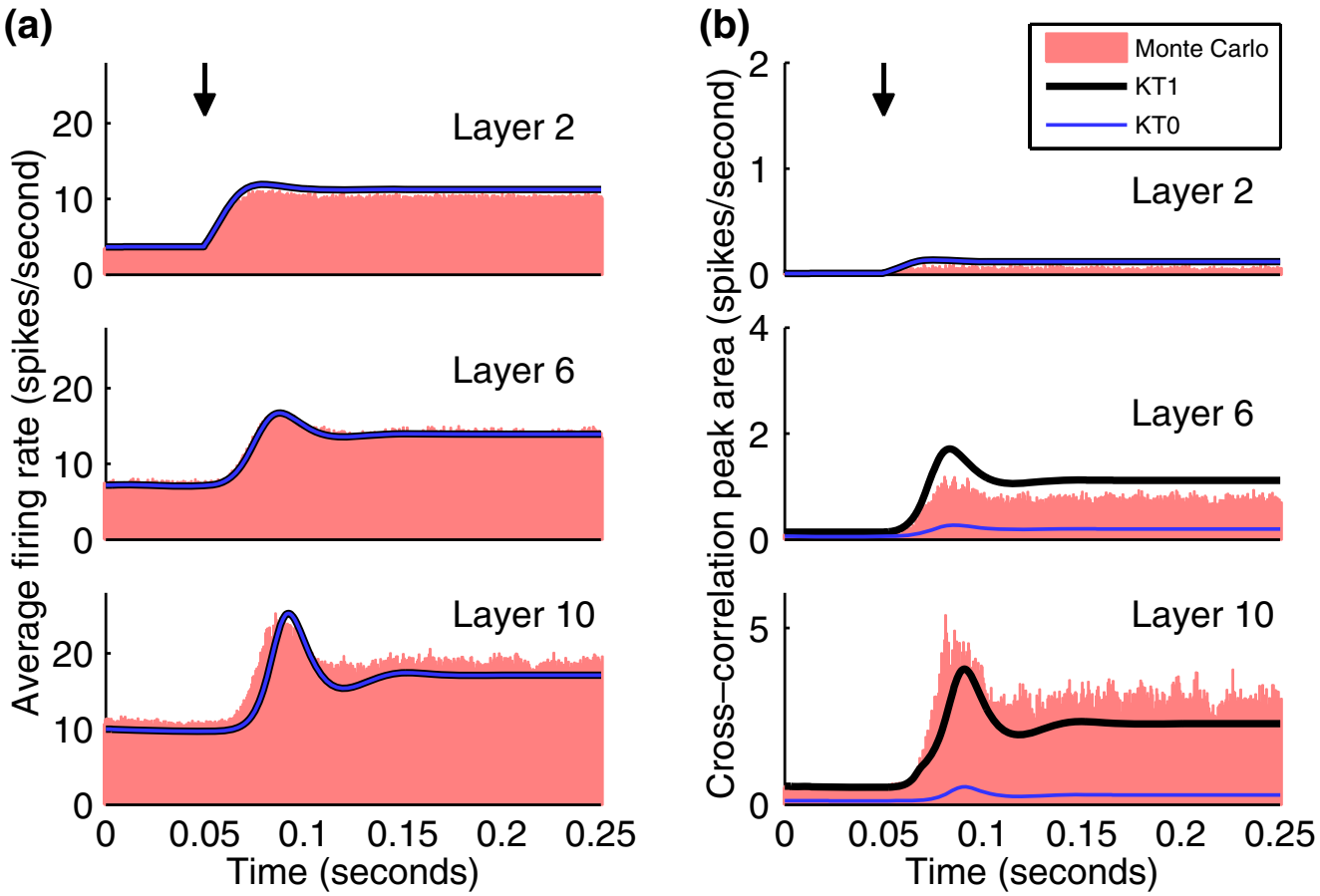

Fig. 10 Comparison of Monte Carlo and kinetic theory results for the network with $\beta = 0.1$ ($N = 100$ in Monte Carlo). Panels as in Fig. 9. For this large fraction of shared connections β, KT1 captures the initial build-up of correlations as shown in layer 6 (overestimating the actual magnitude as expected), but underestimates the increased correlation in deeper layers. KT0 grossly underestimates the correlations. For both methods, the average firing rate is slightly underestimated in deep layers

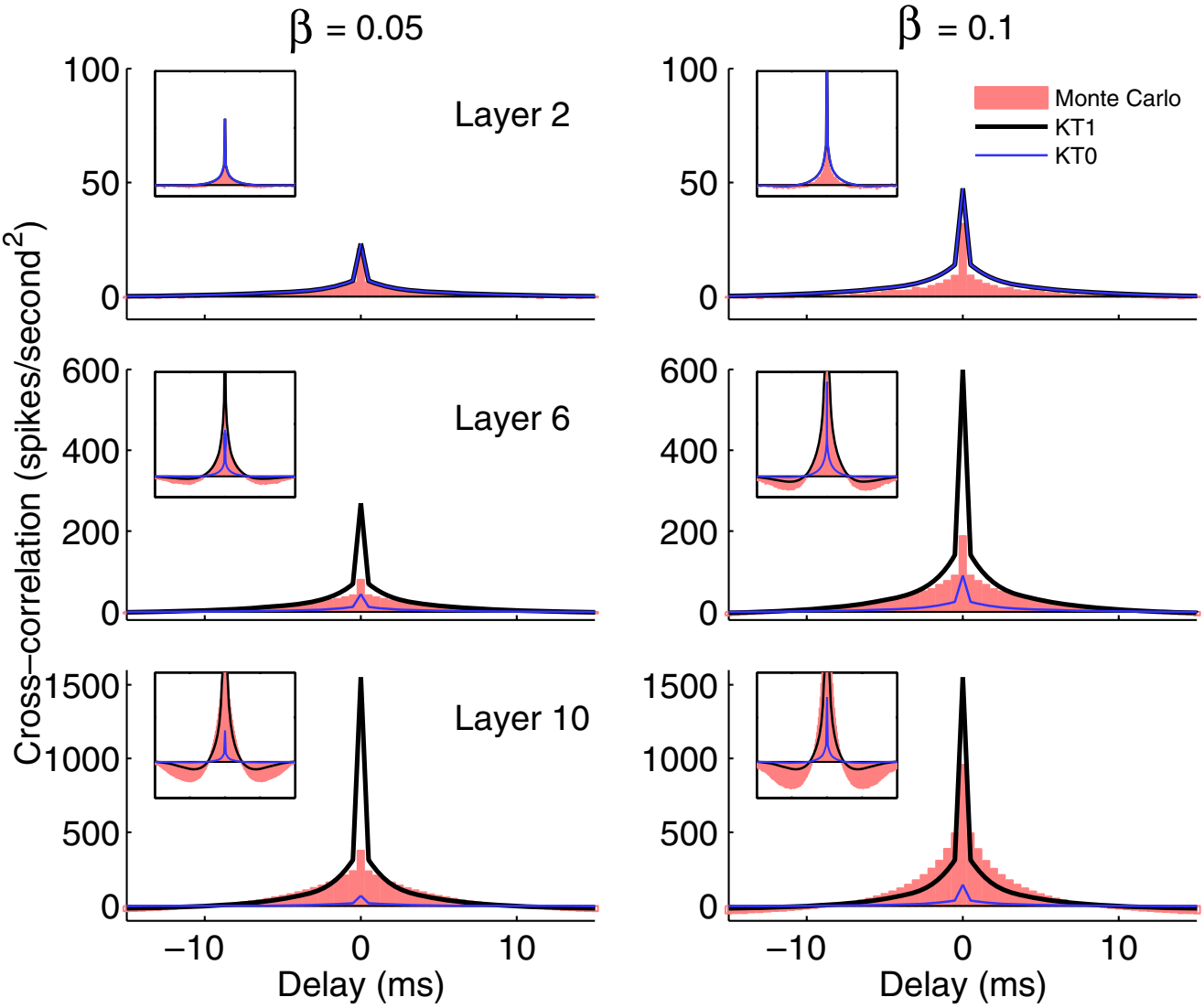

Fig. 11 Comparison of the structure of steady state cross-correlation for layers 2, 6, and 10 of the $\beta = 0.05$ network of Fig. 9 (left column) and the $\beta = 0.1$ network of Fig. 10 (right column). The Monte Carlo and kinetic theory cross-correlations were computed as in Fig. 6(b); in particular, the delta-function component of the kinetic theory correlation was smoothed over a $\Delta t = 0.5$ ms bin centered at the origin. In each panel, the central peak of the cross-correlation, which is used to calculate the peak area $C_{\text{peak}}(t)$, is shown in main plot. For the deeper layers of the $\beta = 0.05$ network and the intermediate layers of the $\beta = 0.1$ network, KT1 overestimates the correlation at zero delay. By layer 10 of the $\beta = 0.1$ network, KT1 no longer overestimates the zero delay correlation and significantly underestimates it at non-zero delay. The insets show the correlation over a larger range of delays to reveal the negative correlation at longer delays, which are not captured by KT1. KT0 uniformly underestimates the correlation by a large margin

we do not expect KT1 to accurately reproduce all the structure of the cross-correlation as a function of delay. Indeed, for the $\beta = 0.05$ network, KT1 grossly overestimates the correlation at zero delay in the deeper layers (left column of Fig. 11). This greater correlation at zero delay explains the overestimate of the peak area $C_{\text{peak}}(t)$ as compared to Monte Carlo. As shown by the insets, KT1 also misses most of the negative correlation at larger delays, although this correlation is not included in the peak area $C_{\text{peak}}(t)$ plotted in Fig. 9(b).

For the $\beta = 0.1$ network, KT1 overestimates the correlation with zero delay only in the intermediate layers. By layer 10, the zero-delay correlation from the Monte Carlo simulations is as large as KT1 correlation despite the fact that KT1 assumes the all the input correlation is at zero delay. KT1 significantly underestimates the correlation at non-zero delay so that the total area in

the peak is well under that of the Monte Carlo, as shown in Fig. 10(b).

The cross-correlation of layer 10 for the $\beta = 0.01$ (i.e., $N = 1{,}000$ for Monte Carlo) and $\beta = 0.2$ (i.e., $N = 50$ for Monte Carlo) networks are shown in Fig. 12. For $\beta = 0.01$, only a small amount of correlation has built up over 10 layers (c.f., 1,000 neuron plots of Fig. 7). As with the $\beta = 0.05$ case, KT1 overestimates the cross-correlation peak area $C_{\text{peak}}(t)$ for all times after stimulus onset (top of Fig. 12(a)) due to an overestimate of small-delay correlation (top of Fig. 12(b)). For the $\beta = 0.2$ network (bottom of Fig. 12), the underestimate of the correlation already seen with $\beta = 0.1$ has become much more dramatic. The KT1 estimate differs little from that of $\beta = 0.1$, although the correlation in the Monte Carlo network doubled. Clearly, the current implementation of the kinetic theory cannot capture the high degree of correlation seen with the higher β networks. Even the correlation at zero delay (bottom of Fig. 12(b)) is substantially underestimated by KT1.

The steady-state results from all four networks are shown in Fig. 13. The average firing rate (left column) is accurately estimated by both KT0 and KT1, except for small underestimates in the deeper layers for the larger βs. For the cross-correlation peak area (right column), KT0 fails to capture even the small correlations of the small β networks. On the other hand, KT1 does a reasonable job estimating (albeit overestimating) the correlation as long as the correlation isn't too large. Since the KT1 estimate of cross-correlation peak area C_{peak} seems to saturate at around 2.4 spikes per second, the correlation estimated by KT1 falls well behind the actual correlation observed in the Monte Carlo networks in the $\beta = 0.1$ and $\beta = 0.2$ networks. By layer 10 for $\beta = 0.1$ and layer 7 for $\beta = 0.2$, the networks appear to be too correlated for the approximations underlying our kinetic theory implementation. We conclude that KT1 captures the build-up of steady-state cross-correlation in feed-forward networks up through moderate levels of correlation but fails in cases with strong correlation.

As a further test of the kinetic theory, we ran additional groups of simulations. We used three different values of expected number of connections: $W^1 = 8$, 10, and 12. For each of these values, we ran two

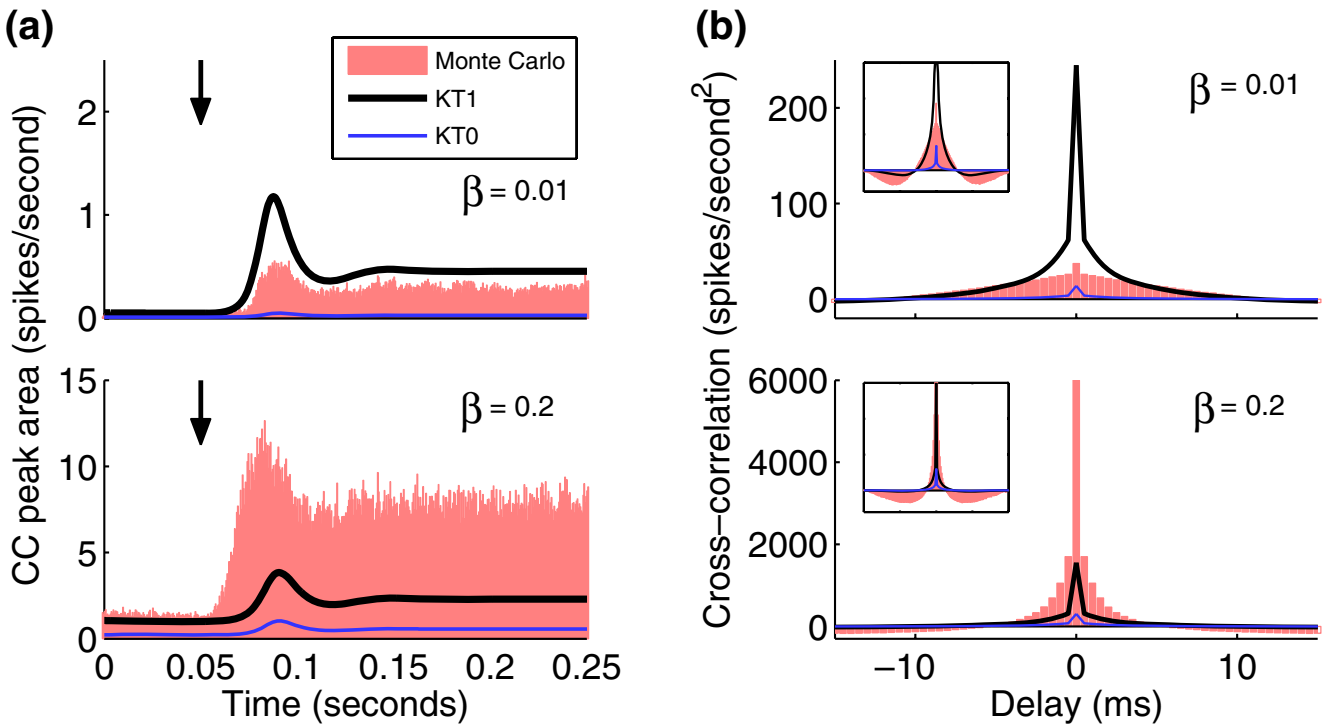

Fig. 12 Comparison of the cross-correlation in layer 10 for the networks with $\beta = 0.01$ ($N = 1{,}000$ for Monte Carlo) and $\beta = 0.2$ ($N = 50$ for Monte Carlo). (**a**) The cross-correlation peak area $C_{\text{peak}}(t)$ is plotted versus time. Panels as in Fig. 9(b). The small correlation in the $\beta = 0.01$ network is slightly overestimated by KT1. The large correlation in the $\beta = 0.2$ network is substantially underestimated by KT1 (**b**). The cross-correlation is plotted versus delay. Panels as in Fig. 11. KT1 overestimates the small-delay correlation for the $\beta = 0.01$ network and uniformly underestimates the correlation for the $\beta = 0.2$ network. KT0 misses the correlation in all cases

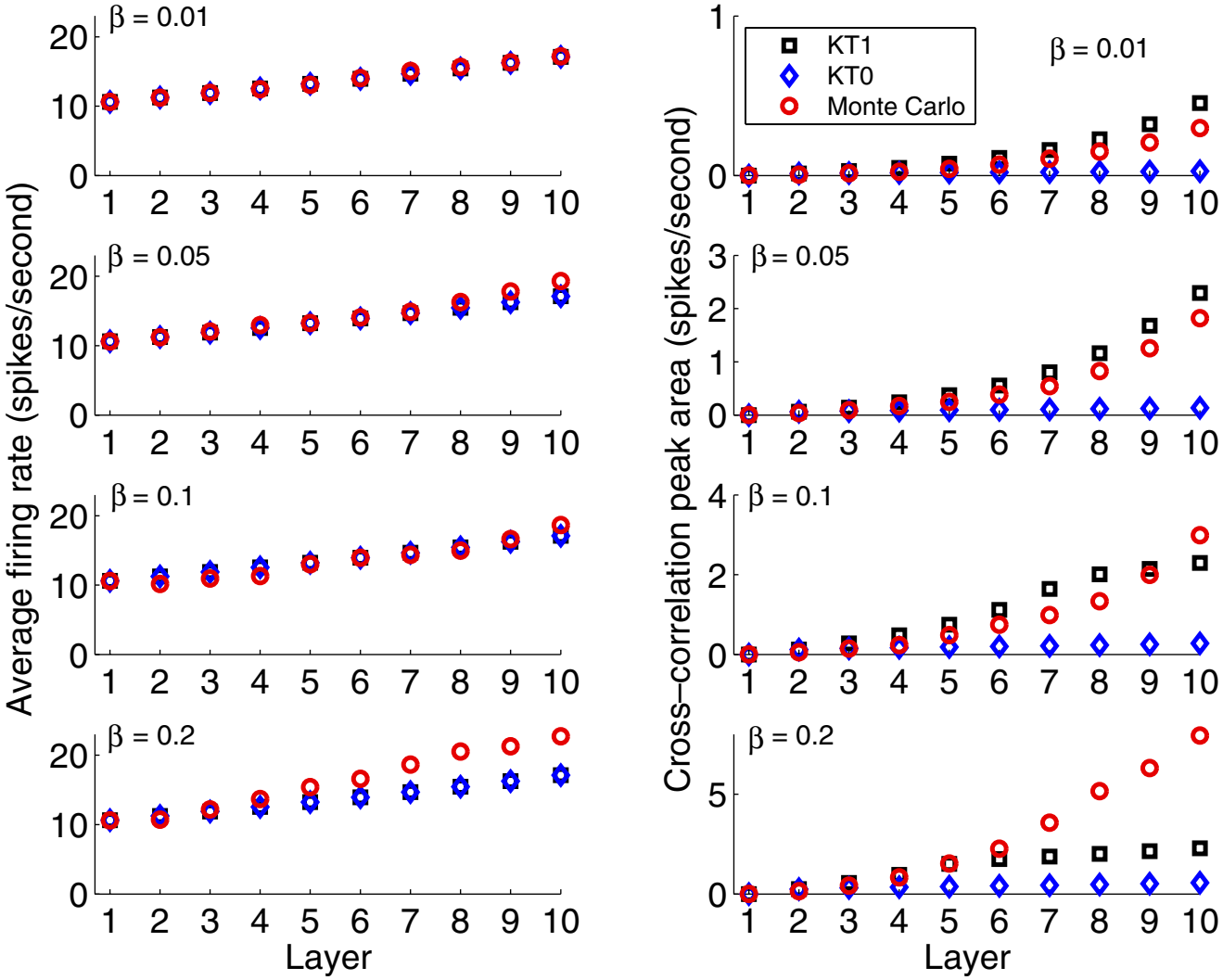

Fig. 13 Comparison of the steady state values of the average firing rate r_{ave} and cross-correlation peak area C_{peak} for all layers of the four tested networks with $\beta = 0.01$, 0.05, 0.1 and 0.2. Both KT1 and KT0 approximate the steady-state firing rate fairly well for all networks. For $\beta \leq 0.05$, KT1 captures the build-up of correlations through all ten layers of the network, though it overestimates the magnitude. For the $\beta = 0.1$ and 0.2, KT1 only captures the initial build-up of correlation in the first layers of the network but fails to estimate the large degree of correlation that occurs in the deeper layers. KT0 severely underestimates all correlations

groups of simulations: one where we set the external input rates $\nu^k_{\text{ind,ext}}$ so that each population fired around 10–15 spikes per second (the "low rate" group) and another where we set the $\nu^k_{\text{ind,ext}}$ so that each population fired around 50–60 spikes per second (the "high rate" group). The simulations shown above were therefore from the $W^1 = 10$, low rate group. For each group, we simulated networks with various β, comparing the KT1 and Monte Carlo results at steady state.

As shown in Fig. 14, KT1 captures the steady state correlation in all networks as long as the correlation isn't too high. For each layer 2 and above (for layer 1, the correlation is zero), we plotted a point corresponding to the steady state correlation C_{peak} as a fraction of the average firing rate r_{ave} calculated by KT1 and Monte Carlo simulations. For C_{peak}/r_{ave} less than about 0.1, the points lie above the diagonal, confirming that the KT1 captures the build-up of correlations in all these networks, slightly overestimating the magnitude. Depending on the average connectivity W^1 and firing rate, KT1 reaches a point where the correlation it can represent saturates at some maximal value. For network layers where the correlation estimated by Monte Carlo simulations exceeded this maximum value, the KT1 limitation lead to underestimation of the correlation.

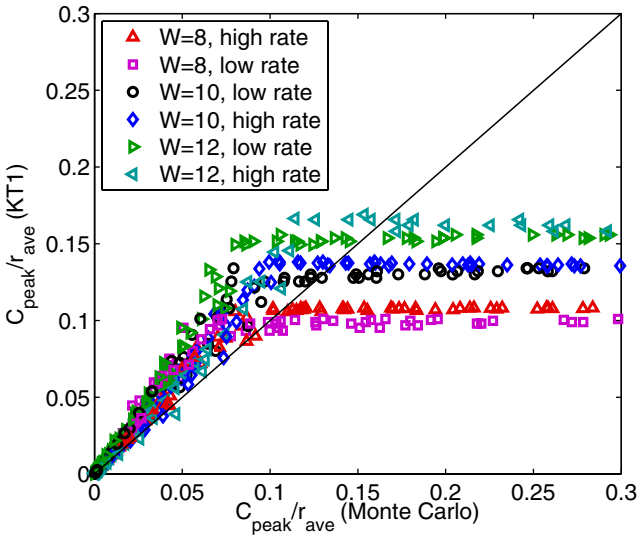

Fig. 14 Comparison of the steady state correlation calculated from KT1 and Monte Carlo for many networks and layers 2 through 10. The cross-correlation peak area C_{peak} is plotted as a fraction of the average firing rate r_{ave}. The KT1 network tends to overestimate the cross-correlation until KT1 saturates at its maximum possible correlation. (Points where the Monte Carlo $C_{\text{peak}}/r_{\text{ave}} > 0.3$ were omitted; in these cases, the KT1 values simply stayed at the saturation point.) For all "low rate" simulations, we set the input to layer to be $\nu^1_{\text{ind,ext}} = 300$ spikes per second, and for all "high rate" simulations, we set $\nu^1_{\text{ind,ext}} = 600$ spikes per second. For the remaining layers $k > 1$, the external input $\nu^k_{\text{ind,ext}} = \nu_0$ varied by networks as follows (all values in spikes per second). $W^1 = 8$: low rate $\nu_0 = 220$, high rate $\nu_0 = 300$. $W^1 = 10$: low rate $\nu_0 = 200$, high rate $\nu_0 = 200$. $W^1 = 12$: low rate $\nu_0 = 175$, high rate $\nu_0 = 110$

3.2.3 The sufficiency of second order connectivity statistics

We are developing our kinetic theory approach based on the hypothesis that second order statistics of neuronal activity are sufficient to describe much of the behavior of neuronal networks (Schneidman et al. 2006; Shlens et al. 2006; Tang et al. 2008; Yu et al. 2008). We do not test this hypothesis directly here, as we have been examining output statistics of only first and second order (average firing rate and cross-correlation). Even so, we can indirectly test one implicit assumption of the approach: that second order connectivity statistics (expected number of inputs W^1 and fraction of shared inputs β) are sufficient to determine the second order statistics of the network output. We can test this hypothesis by simulating networks with different types of connectivity patterns that have the same second order connectivity statistics but differ in third and higher order statistics.

In Appendix B, we calculate the statistics W^1 and β for networks with prescribed outgoing degree distributions and with incoming degree distributions that are equivalent to those of the random networks described above. Then, we generated multiple ten layer feed-forward networks with $W^1 = 10$ and various values of β between 0 and 0.2. We simulated the networks to the same input conditions as in the $W^1 = 10$, low rate, networks described above and calculated the steady-state values of the average firing rate r_{ave} and cross-correlation peak area C_{peak} for layer 10.

For each set of network parameters, we performed two types of Monte Carlo simulations. First, we randomly generated a single network and simulated the response of this fixed network to $400\max(1, 1000/N)$ presentations of the input, where N is the number of neurons per layer. This first type of simulation corresponds to the Monte Carlo simulations employed above. For the second type of Monte Carlo simulation, we simulated the network response to the same number of presentations of the input, but this time, for each input presentation, we regenerated a new realization of the network. By rewiring the network for each realization, we averaged over the fluctuations due to particular network configurations so that we could better estimate how the output statistics depend on the type of network. Note that the kinetic theory networks are designed to capture the behavior of the average network with particular network statistics as represented by the latter type of Monte Carlo simulations.

We simulated Monte Carlo networks with seven different degree distributions. The first network class was composed of random networks, as described above (which have a binomial degree distribution). The second consisted of networks with outgoing degree distributions that followed a power law. Then, we simulated networks with a power-law outgoing degree distributions, except that we truncated the maximum outgoing degree at different values: 100, 500, 2,000, and 5,000. (Clearly, these differed from the networks with the unmodified power-law distribution only if the number of neurons per layer N was larger than the cutoff.) Lastly, we simulated networks with outgoing degree-distributions that were Gaussian.

As described in Appendix B, each class of networks has a single free parameter once the layer size N was specified. This parameter was set to match the condition that the expected number of incoming connections was $W^1 = 10$. The value of that parameter determined the fraction of shared input β. In this way, for each class of network, β was a function of N. Since this function depended on the class of network, we could obtain different values of β for each N. By examining

the output statistics r_{ave} and C_{peak} evaluated for the steady state of layer 10, we could investigate if these output statistics were primarily determined by β (as we hypothesize in the formulation of the kinetic theory equations) or by the layer size N (as Fig. 7 seemed to indicate).

The results of these simulations are shown in Fig. 15. If we look only at networks where we regenerated the network circuitry for each realization (filled symbols), we see that both the average firing rate r_{ave} (Fig. 15(a)) and the cross-correlation peak area C_{peak} (Fig. 15(b)) are very well approximated as functions of β. (The

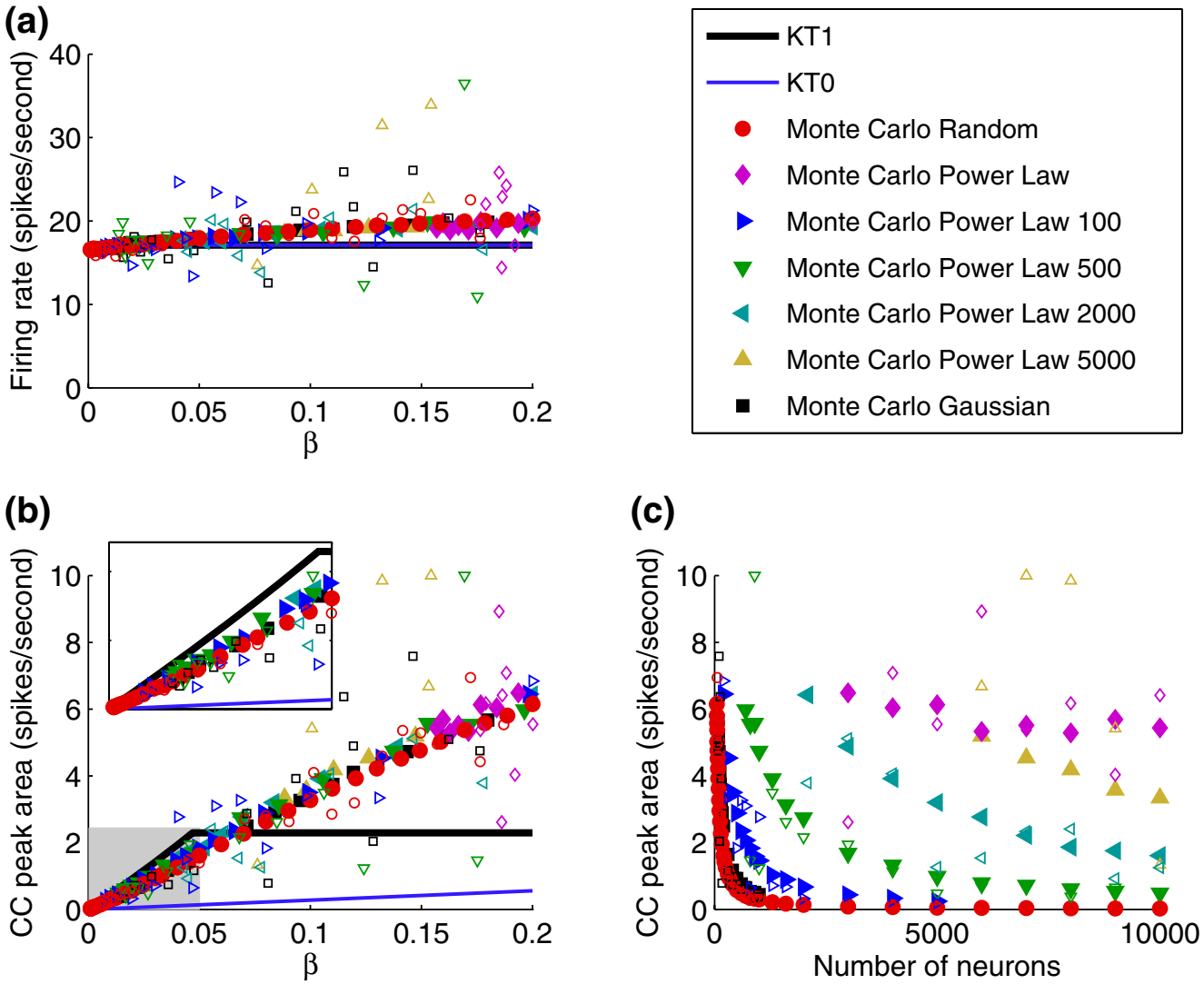

Fig. 15 Steady state values of average firing rate r_{ave} and cross-correlation peak area C_{peak} in layer 10 for different classes of networks. *Filled symbols* correspond to Monte Carlo simulations of averaged networks, where the network connectivity was re-generated at each realization. *Open symbols* correspond to a simulations of a single fixed network of the same network class as the corresponding filled symbol. The number for the power law networks indicates the maximum outgoing degree allowed. (**a**) The firing rate for averaged networks increases modestly with β, and the fixed network values are more scattered. The KT1 and KT0 results are similar to the averaged networks, though they show little increase with β. (**b**) The cross-correlation peak area C_{peak} for averaged networks appears to be nearly a function of β, as the *filled symbols* lie along a single curve. *Open symbols* are scattered around the *filled symbols*, indicating the variability observed among the fixed networks. *Inset* is detail of results for $\beta \leq 0.05$ (*shaded region*). In this range, KT1 is a good approximation of the averaged network results, though the magnitude is overestimated. For larger β, KT1 does not show the increase in C_{peak} with β. KT0 fails to capture C_{peak} even for small β. For display purposes, C_{peak} was truncated to 10 for two points. (**c**) The cross-correlation peak area C_{peak} is not well approximated as a function of layer size N. For any value of N, the correlation depends strongly on the type of network. To correspond to panel (**b**), only points with $\beta \leq 0.2$ are shown

open symbols corresponding to simulations of fixed networks have a large spread around the filled symbols.) Moreover, for $\beta \leq 0.05$, the functions of β given by the filled symbols are close to that predicted by KT1 (though the KT1 curve overestimates the magnitude the cross-correlation). Importantly, even for large β the filled symbols nearly lie along a curve, indicating that the second order connectivity statistics are sufficient to determine the second order output statistics. Although the KT1 curve strongly deviates from the Monte Carlo curve for large β, the fact that the Monte Carlo points lie along a single curve indicates that it may be possible for a kinetic theory based on W^1 and β to capture the full range of correlations (see Section 4).

In contrast, the plot of C_{peak} versus N (Fig. 15(c)) indicate that layer size N is not a good predictor of the correlation if the class of network is not specified. Even the filled symbols have a large spread for all layer sizes. If one restricts attention to a particular network class, then the filled symbols do fall along a single curve, which is due to the fact that β is a function of N when the network class is fixed. These results clearly demonstrate that the fraction of shared input β, not layer size N, is critical for determining the build-up of correlations in feed-forward networks.

As a final illustration of the fact that the first and second order connectivity statistics, not network size, determine the network behavior, we created four different networks with vastly different sizes and the same connectivity statistics. In each case, we created networks to match the connectivity statistics $W^1 = 10$ and $\beta = 0.05$ of the network from Fig. 9. If we used a power law outgoing degree distribution capped at 5,000, we needed $N = 17{,}500$ neurons per layer to reduce β down to 0.05. Capping the outgoing degree at 2,000 and 500 reduced the layer size to $N = 8{,}350$ and $N = 2{,}750$, respectively. In comparison, the random network of Fig. 9 had only $N = 200$ neurons per layer. For each network, we stepped up the input rate at $t = 0.05$, using the input rates for Fig. 9. We presented this input 2,000 times and regenerated the circuitry for each realization.

The neuronal output of layer 10 of each network is shown in Fig. 16. The activity of each network is similar, indicating the first and second order connectivity statistics did determine most of the behavior. Some minor differences are that the random network had slightly lower steady state correlation and some of the power law networks appeared to have a larger transient correlation in response to the input step. Hence, although the second order connectivity statistics did not determine every detail of the neuronal activity, the connectivity statistics W^1 and β did capture the essential features of the connectivity needed to describe most of the second order statistics of the network activity.

4 Discussion

We have developed a kinetic theory approach that captures the build-up of correlations in feed-forward neural networks as long as the cross-correlation does not become too large. We demonstrated that although approximating delayed correlation as instantaneous correlation resulted in an overestimate of the magnitude of output cross-correlation, it accurately represented how the correlations increased with respect to layer and with respect to fraction of shared inputs in the connectivity structure.

4.1 Sufficiency of second order connectivity

Our goal is to use a second order kinetic theory description to describe the behavior of neuronal networks. We base this goal on the assumption that describing neuronal activity via second order statistics will be sufficient to explain much of the behavior of the networks (c.f., Schneidman et al. 2006; Shlens et al. 2006; Tang et al. 2008; Yu et al. 2008). In order to derive equations by which to couple the population densities of the kinetic theory, we distilled the network connectivity patterns between two populations into first and second order statistics. Our hypothesis was that these first and second order connectivity statistics would be sufficient to specify the resulting first and second order statistics of the neuronal activity. It is not obvious that such a hypothesis should be true, and we expect that higher order statistics will have some effect. For example, the second order connectivity statistic β does have a small effect on the first order output statistic r_{ave}, as shown by the slight increase of the filled dots with β in Fig. 15(a). The fact that we demonstrated that the cross-correlation peak area is primarily determined by β (for fixed first order statistic W^1 and fixed input rates) is encouraging support of the notion that our kinetic theory approach may be able to capture the fundamental mechanisms underlying the emergence and propagation of correlations.

One caveat should be stressed. In all the Monte Carlo networks we used to generate Fig. 15, we varied only the *outgoing* degree distribution of the nodes. We did not, for example, create networks with power law incoming degree distributions. Especially since we do not include inhibition, we could not include neurons that had 100 times more inputs than average. If we did,

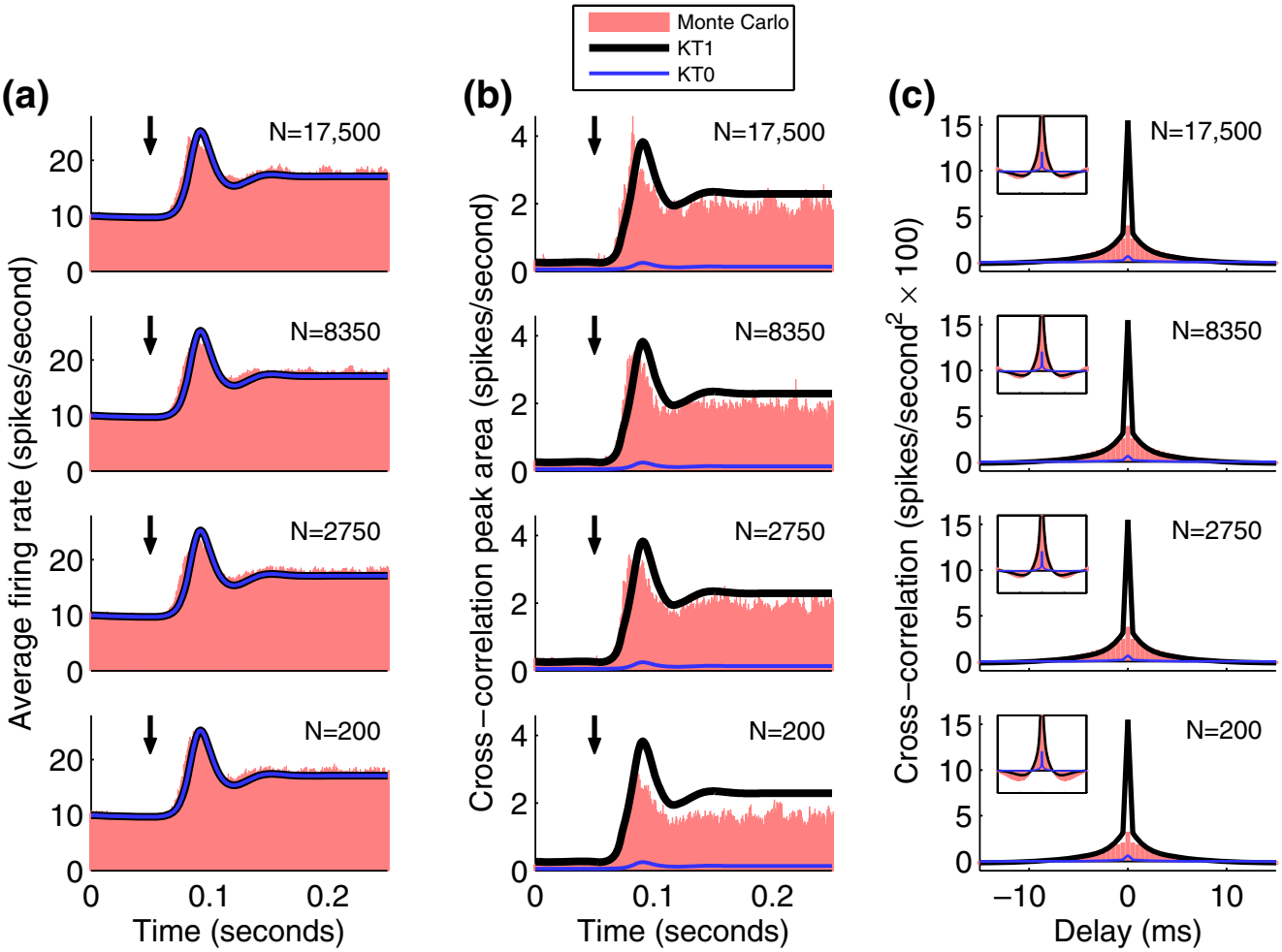

Fig. 16 Comparison of layer 10 results from four different networks with different numbers of neurons but the same connectivity statistics ($W^1 = 10$ and $\beta = 0.05$). The top row is a network with $N = 17{,}500$ neurons per layer and a power law outgoing degree distribution capped at a maximum outgoing degree of 5,000. In the *second* and *third row*, the power law degree distribution was capped at 2,000 and 500, respectively, and the number of neurons per layer was 8,350 and 2,750, respectively. The *fourth row* is a random network with $N = 200$ neurons per layer. In each case, network activity was obtained in response to 2,000 realizations of same input as for Figs. 9–13, and the network circuitry was regenerated for each realization. Except for this circuitry regeneration, the fourth row is the same as the bottom row of Fig. 9 and the bottom left of Fig. 11. The kinetic theory results are simply replotted for each row. (**a**) Average firing rate $r_{\text{ave}}(t)$ plotted as in Fig. 9(a). (**b**) Cross-correlation peak area $C_{\text{peak}}(t)$ plotted as in Fig. 9(b). (**c**) Steady state cross-correlation structure plotted as in Fig. 11. Despite the vastly differing network size, the network output is similar because for each network class, we chose the network size to match the connectivity statistics $W^1 = 10$ and $\beta = 0.05$

those neurons would have fired at unreasonable rates. Hence, in all networks, we always assigned postsynaptic targets randomly.

4.2 Related kinetic theory and correlation analyses

Our kinetic theory approach is based on the population density formulation of interacting neuronal populations introduced by Knight, Sirovich, and colleagues (Knight et al. 1996; Omurtag et al. 2000b; Sirovich et al. 2000; Omurtag et al. 2000a; Knight 2000; Casti et al. 2002; Sirovich et al. 2006; Sirovich 2008) that was further developed by Tranchina and colleagues (Nykamp and Tranchina 2000, 2001; Haskell et al. 2001; Apfaltrer et al. 2006). Although there are many examples of using kinetic theory to model neuronal networks (Abbott and van Vreeswijk 1993; Barna et al. 1998; Brunel and Hakim 1999; Gerstner 2000; Câteau and Fukai 2001; Hohn and Burkitt 2001; Mattia and Del Giudice 2002; Moreno et al. 2002; Meffin et al. 2004; Câteau and Reyes 2006; Doiron et al. 2006; Cai et al. 2006; Huertas and Smith 2006), most approaches do not explicitly represent correlations among neurons but instead assume

each neuron in a population is an independent sample from the distribution.

A notable exception is upcoming work by de la Rocha et al. (2008) where they also develop a kinetic theory based on a pair of neurons with correlated input. In their case, they assume the inputs are Gaussian white noise and are even able to derive an analytical formula for the output cross-correlation. Their goal is also to study how correlated activity propagates over multiple layers of a network.

There have been many studies characterizing how correlated inputs to uncoupled neurons lead to correlated outputs (Dorn and Ringach 2003; Galán et al. 2006; Svirskis and Hounsgaard 2003; Moreno-Bote and Parga 2006; Binder and Powers 2001; Shadlen and Newsome 2001). Recent results have shown how under certain circumstances, the amount of input correlation that is transfered to output correlation depends primarily on the firing rate (de la Rocha et al. 2007), and one can further characterize this relationship between input and output correlation (Shea-Brown et al. 2008). One additional challenge we have faced in our kinetic theory implementation is how to transform the output correlation of a presynaptic population into the input correlation of its postsynaptic population.

Our application of kinetic theory to correlations in feed-forward networks was motivated by experimental observations of the emergence of sustained synchrony in such networks (Reyes 2003) and applications of kinetic theory to understand their properties (Câteau and Reyes 2006; Doiron et al. 2006). The authors discovered typical kinetic theory implementations miss the build-up of sustained synchrony. Although an ad hoc finite-size correction (Brunel and Hakim 1999; Mattia and Del Giudice 2002; Hohn and Burkitt 2001) can restore elements of this synchrony (Doiron et al. 2006), it does not explicitly model the correlations that underlie the synchrony.

Our use of the term kinetic theory is motivated by similarities to the kinetic theory of gases and plasmas. However, our approach differs from the kinetic theory of gases and plasmas in two main ways. First, in our system, the particles (neurons) are inherently stochastic since we model their inputs as Poisson processes. Second, in our feed-forward network model, we view each population as containing non-interacting neurons. Consequently, the evolution equation for the second order density ρ does not depend on higher order correlations. In standard kinetic theory approaches, one develops a BBGKY (Bogoliubov–Born–Green–Kirkwood–Yvon) moment hierarchy (Ichimaru 1973; Nicholson 1992), and then makes an approximation to truncate the hierarchy and obtain a closed system of equations. For example, this was the approach used for a kinetic theory model of coupled oscillators by Hildebrand et al. (2007). Our feed-forward model does not require such a moment closure assumption to obtain an evolution equation for ρ. Instead, we must make a moment closure assumption to determine the input to each population because the evolution of the second order density depends on higher order moments of the input. For this initial work, we used a simple truncation of ignoring triplet or higher order synchronous input. We propose an improved closure below.

4.3 Extending the approach to higher correlations

We have demonstrated that our current kinetic theory implementation (KT1) works well up to moderate levels of correlation but that it fails to capture the network behavior once the correlation becomes too large. The result is understandable given the assumptions we invoked to derive the network equations in Section 2.5. In particular, the kinetic theory equations (2) include input rates representing only independent input to a single neuron and synchronous arrival of a single input to each of a pair of neurons. The equations neglect the possibility that two (or more) synchronous inputs could arrive at the same neuron. Such an event would lead to a voltage jump of double (or larger) size. A double jump is more effective in driving a neuron than two independent jumps of normal size. Since such double jumps become more common with increased network synchrony, they are presumably behind the increase in firing rate $r_{\text{ave}}(t)$ with β that is not captured by KT1 (Fig. 15(a)).

The double-sized jumps have an even more profound effect on cross-correlation because the double jumps in one neuron's voltage could occur simultaneously with jumps (or double jumps) in another neuron's voltage. These synchronous jumps of double (or larger) size lead to correlations that are not captured by our kinetic theory equations, as they are limited to synchronous jumps of normal size. The saturation to maximal possible correlation in Figs. 14 and 15(b) occurs when the expression (13) for the synchronous input rate ν_{syn} becomes larger than the total input from presynaptic populations. To ensure that the independent input rate ν_{ind} given by Eq. (14) is not smaller than the external input rate ν_{ext} (which we know is independent), we truncate ν_{syn} to the total input from presynaptic populations. For the given average firing rate and the given external input rates, it is simply impossible for the kinetic theory equations to yield higher correlation than observed in Figs. 14 and 15(b). By looking at single populations with prescribed input rates ν_{ind} and ν_{syn},

we confirmed that the saturation points of our kinetic theory implementation correspond to the point where all input to the population is synchronous except the independent input corresponding to the external input rate ν_{ext}.

To extend the validity of our kinetic theory equations to higher levels of correlation, we must augment the equations with terms corresponding to double jumps. We would need to add terms corresponding to independent double jumps in one neuron, synchronous double jumps in both neurons, and double jumps in one neuron that were synchronous with single jumps in the other. In this way, we could fully represent the pattern of inputs to a pair of neurons that could result from a pair of presynaptic neurons firing synchronously.

Such an augmentation of the equations would not account for the input patterns from a highly synchronous presynaptic population. In the highly synchronous case, three or more neurons may be highly likely to fire simultaneously. Such firing patterns will lead to combinations of double or larger sized voltage jumps that cannot be captured by an analysis of just pairs of presynaptic neurons firing synchronously. Although it may naively appear that we need to represent third or higher order statistics to capture such firing patterns, one can still infer the presence of higher order firing patterns from second order statistics.

Imagine, for example, that a presynaptic population contained three neurons with identical firing rates and pairwise correlation, as assumed by our kinetic theory. If the correlation between each pair was high, then it would be highly likely that each pair was either silent or firing together (recall, we are ignoring delayed correlation). Since in this extreme case, it would be unlikely to find a pair where one neuron is firing and another is silent, we immediately observe that it would be rare to have only one out of the three neurons fire or have two of the three neurons fire without the remaining neuron joining in the firing. The likely states would be that either all three neurons are silent or all three neurons are firing together.

This extreme example illustrates some of the implications of second order statistics on the likelihood of observing higher order firing patterns. We did not need to assume anything special about the third order statistics to infer the likelihood of third order firing patterns. The likelihood of triplet firing was simply a consequence of the large pairwise correlation. In less extreme cases with lower pairwise correlation and more neurons, there is a lot more flexibility of what higher order statistics could correspond prescribed second order statistics. However, if one does not want to prescribe additional structure on the higher order statistics, one can infer predictions about higher order statistics by assuming minimal structure using maximum entropy estimates of the higher order statistics (Jaynes 1957). Such methods were behind efforts to determine if one needed to assume higher order structure in neuronal activity in order to predict firing patterns among simultaneously recorded neurons (Schneidman et al. 2006; Shlens et al. 2006; Tang et al. 2008; Yu et al. 2008). For point processes such as the firing of neurons, such calculations would be based on the entropy rates of point processes (McFadden 1965). For example, one could approximate the rates at which three or more neurons fire synchronously as those rates that maximize the entropy rate of the joint firing of those neurons.

The implications of second order statistics on higher order statistics becomes an important consideration for designing our second order kinetic theory approach. As pairwise correlations increase, so does the likelihood that more than two presynaptic neurons may fire simultaneously. In this case, not only do the double jumps described above become prevalent, but also triple and larger jumps start to have an effect. Hence, another way to improve the kinetic theory performance under high correlation is to use maximum entropy rate methods to estimate the rate of synchronous firing by more than two neurons from the quantities $r_{\text{ave}}(t)$ and $\tilde{r}_{\text{syn}}(t)$ and include the effect of such events in the evolution of the postsynaptic populations.

4.4 Including autocorrelations

In our kinetic theory formulation, we assumed the input to each neuron was a modulated Poisson process, completely ignoring any autocorrelations in the input. Such autocorrelation in the firing times of neurons are clearly present even in our simplified integrate-and-fire model, as a neuron needs time to integrate up to threshold after firing. Moreover, since it is well-known that the output of neurons is not Poisson (Stevens and Zador 1998; Shinomoto et al. 2003; Salinas and Sejnowski 2002), it is clear that our Poisson assumption is unrealistic. We suspect that such a Poisson assumption has decreased the accuracy of our kinetic theory approach.

Recent kinetic theory approaches have included autocorrelations of the input using colored noise (Câteau and Reyes 2006; Doiron et al. 2006) or a renewal process description (Ly and Tranchina 2008). We could incorporate such autocorrelations along with the cross-correlations. Including such autocorrelations would require the addition of two more variables to our

population density (for example, the times since neuron 1 and neuron 2 received their last inputs). Those same variables could also be used to include cross-correlations at non-zero delays, leading to a more complete description of the second order statistics in the neuronal activity in terms of correlated renewal processes. Hence, this extension may reduce the overestimate of correlation that we currently observe from our method of collapsing delayed correlation to make it instantaneous. Unfortunately, simulating the evolution of a four-dimensional population density function would be computationally expensive. To make their numerical solution more tractable, we would need to search for techniques to reduce the dimension, searching along the lines, for example, of a rescaling technique used to approximate a colored noise process by a white noise process (Moreno et al. 2002).

4.5 Fast numerical methods

The focus of this work has been to explore how well one could capture the emergence and propagation of correlation with a kinetic theory description that represents some of the second order statistics of neuronal activity and connectivity patterns. At this point, we have not developed a fast numerical method to quickly solve the equations (2). Fortunately, a wide range of techniques have been developed for efficient numerical solution of such equations.

One promising option to speed up the computations is recently developed dynamic basis set techniques for efficient simulation of this class of problems (Knight 2000; Mattia and Del Giudice 2002). This method relies on the observation that the state of a system such as $\rho(v_1, v_2, t)$ is typically concentrated in a relatively small subspace. One constructs a dynamic basis set of eigenfunctions and can reduce computational complexity by tracking only a small number of eigenmodes. Such an approach has been successfully used with two-dimensional integrate-and-fire models (Apfaltrer et al. 2006), and may be a good method to speed up the higher-dimensional densities involving correlations. Operator splitting is another technique to speed up simulations (Apfaltrer et al. 2006) that could be employed with our model.

Another way to speed up the solution of Eq. (2) is to turn the integro-differential equation into a diffusion equation under the assumption that the jump size A is small. The partial differential equation can be solved more quickly because one obtains a sparser matrix when discretizing the derivatives with respect voltage. However, the diffusion approximation loses accuracy as the jump size becomes large. For this reason, the diffusion approximation may be inaccurate when the correlation is high and double-sized (or larger) voltage jumps become common. We plan to investigate the ability of the diffusion approximation to capture highly correlated activity in the future.

4.6 A tool to analyze network behavior and connectivity

Our goal for this second order kinetic theory approach is a tool with which to investigate the consequences of network structure on network behavior. We are aiming for a method that one can use to distill the connectivity down to its key features and to study how these features influence the network behavior. Although the development of the tool is still in its early stages (we haven't yet addressed recurrent connections within a population), it has shown promise that it can capture basic aspects of the behavior of second order statistics in feed-forward networks. If one could parameterize network connectivity by second order statistics and use the kinetic theory tool to explore their consequences on second order statistics of neuronal activity, this simplified description may help uncover key network parameters underlying network behaviors.

Already at these initial stages, we have gained some insight into the network parameters that underlie the build-up of correlations. Previous studies (Doiron et al. 2006) have concluded that network size may be the critical factor in determining this behavior. Our kinetic theory analysis suggested that it was the fraction of shared input parameter rather than network size that played the key role. Simulations of networks with different higher order connectivity statistics provided convincing evidence supporting the kinetic theory prediction.

To implement the kinetic theory analysis, one needs methods to determine the second order connectivity patterns at the level of a population coarse-graining. One would like to know what classes of neurons project onto a neuron of a given class (our first order statistic W^1) and what classes of neurons project common input connections onto pairs of neurons of a given class (our second order statistic $W^2 = \beta W^1$). One of us has recently developed a connectivity analysis (Nykamp 2005, 2007a, b) that contains ambiguity that could be at the same level as the population grouping. Although this connectivity analysis is designed to distinguish common input (even originating from unmeasured neurons) from causal connections among a set of measured neurons, more work needs to be done to identify the classes

of the common input neurons. With that extension, the connectivity analysis may be one way to determine the second order statistics of the connectivity needed for the kinetic theory analysis. A tool to estimate second order connectivity and a tool to explore the consequences of second order connectivity could prove a powerful combination for probing basic properties of neural circuits and exploring the link between connectivity patterns and network behavior.

Acknowledgements This work was supported in part by NSF grant DMS 0719724 (DQN) and NIH training grant R90 DK71500 (CYL). We thank Dan Tranchina, Brent Doiron, Michael Buice, Carson Chow, and Hide Câteau for helpful discussions.

Appendices

A Method for solving the kinetic theory equations

The first step in solving the kinetic theory equations (2) is to rewrite them in conservative form, i.e., divergence form $\frac{\partial \rho}{\partial t} = -\nabla \cdot \mathbf{J}$, where $\mathbf{J}$ is a flux density. The terms describing the advection due to the leak current are already the divergence of a flux density. We need to rewrite the integrals corresponding to the voltage jumps in response to excitatory input. Recall that $F_A(x)$ is the complementary cumulative distribution function and $f_A(x)$ is the probability density of the random jump size A, so that $\frac{\partial F_A}{\partial x} = -f_A(x)$. Applying this identity and the fundamental theorem of calculus, we obtain the following equalities. We rewrite the terms due to independent input as

$$\begin{aligned}
&\int_{v_{\text{reset}}}^{v_1} f_A(v_1-\theta_1)\rho(\theta_1,v_2,t)\mathrm{d}\theta_1 - \rho(v_1,v_2,t)\\
&\quad = -\frac{\partial}{\partial v_1}\int_{v_{\text{reset}}}^{v_1} F_A(v_1-\theta_1)\rho(\theta_1,v_2,t)\mathrm{d}\theta_1,\\
&\int_{v_{\text{reset}}}^{v_2} f_A(v_2-\theta_1)\rho(v_1,\theta_2,t)\mathrm{d}\theta_2 - \rho(v_1,v_2,t)\\
&\quad = -\frac{\partial}{\partial v_2}\int_{v_{\text{reset}}}^{v_2} F_A(v_2-\theta_2)\rho(v_1,\theta_2,t)\mathrm{d}\theta_2, \qquad (15)
\end{aligned}$$

The integrals involving F_A are probability flux densities analogous to those defined in Nykamp and Tranchina (2000).

The jumps due to synchronous input are a little more complicated. There are many ways to write them in conservative form. Since the evolution of ρ is symmetric in v_1 and v_2, we kept the equation symmetric by dividing the diagonal jumps into a symmetric pair of horizontal and vertical jumps.

$$\begin{aligned}
&\int_{v_{\text{reset}}}^{v_1}\int_{v_{\text{reset}}}^{v_2} f_A(v_1-\theta_1)\,f_A(v_2-\theta_2)\rho(\theta_1,\theta_2,t)\mathrm{d}\theta_1\mathrm{d}\theta_2\\
&\qquad -\rho(v_1,v_2,t)\\
&\qquad = -\frac{1}{2}\frac{\partial}{\partial v_1}\Bigg(\int_{v_{\text{reset}}}^{v_1} F_A(v_1-\theta_1)\rho(\theta_1,v_2,t)\mathrm{d}\theta_1\\
&\qquad\qquad +\int_{v_{\text{reset}}}^{v_1}\int_{v_{\text{reset}}}^{v_2} F_A(v_1-\theta_1)\,f_A(v_2-\theta_2)\\
&\qquad\qquad \times\rho(\theta_1,\theta_2,t)\mathrm{d}\theta_2\mathrm{d}\theta_1\Bigg)\\
&\qquad -\frac{1}{2}\frac{\partial}{\partial v_2}\Bigg(\int_{v_{\text{reset}}}^{v_2} F_A(v_2-\theta_2)\rho(v_1,\theta_2,t)\mathrm{d}\theta_2\\
&\qquad\qquad +\int_{v_{\text{reset}}}^{v_2}\int_{v_{\text{reset}}}^{v_1} F_A(v_2-\theta_2)\,f_A(v_1-\theta_1)\\
&\qquad\qquad \times\rho(\theta_1,\theta_2,t)\mathrm{d}\theta_1\mathrm{d}\theta_2\Bigg). \qquad (16)
\end{aligned}$$

Although these integrals do not correspond to physical horizontal and vertical jumping of the voltage, we view their formulation simply as an intermediate step to developing a numerical scheme to solve the original Eq. (2).

As a result, we obtain the following integro-differential equation:

$$\begin{aligned}
\frac{\partial\rho}{\partial t}(v_1,v_2,t) &= -\nabla\cdot\mathbf{J}(v_1,v_2,t)+\delta(v_1-v_{\text{reset}})J_{\text{reset},1}(v_2,t)\\
&\quad +\delta(v_2-v_{\text{reset}})J_{\text{reset},2}(v_1,t)\\
&\quad +\delta(v_1-v_{\text{reset}})\delta(v_2-v_{\text{reset}})J_{\text{reset},3}(t), \qquad (17)
\end{aligned}$$

where

$$\begin{aligned}
\mathbf{J}(v_1,v_2,t) &= \mathbf{J}_{\text{leak}}(v_1,v_2,t)+\mathbf{J}_{\text{ind}}(v_1,v_2,t)+\mathbf{J}_{\text{syn}}(v_1,v_2,t),\\
\mathbf{J}_{\text{leak}} &= (J^1_{\text{leak}},J^2_{\text{leak}}),\ \mathbf{J}_{\text{ind}} = (J^1_{\text{ind}},J^2_{\text{ind}}),\\
\mathbf{J}_{\text{syn}} &= (J^1_{\text{syn}},J^2_{\text{syn}}),\\
J^1_{\text{leak}}(v_1,v_2,t) &= -\frac{v_1-Er}{\tau}\rho(v_1,v_2,t),\\
J^1_{\text{ind}}(v_1,v_2,t) &= \nu_{\text{ind}}(t)\int_{v_{\text{reset}}}^{v_1} F_A(v_1-\theta_1)\rho(\theta_1,v_2,t)\mathrm{d}\theta_1,\\
J^1_{\text{syn}}(v_1,v_2,t) &= \frac{1}{2}\nu_{\text{syn}}(t)\Bigg(\int_{v_{\text{reset}}}^{v_1} F_A(v_1-\theta_1)\rho(\theta_1,v_2,t)\mathrm{d}\theta_1\\
&\quad +\int_{v_{\text{reset}}}^{v_1}\int_{v_{\text{reset}}}^{v_2} F_A(v_1-\theta_1)f_A(v_2-\theta_2)\\
&\quad \times\rho(\theta_1,\theta_2,t)\mathrm{d}\theta_2\mathrm{d}\theta_1\Bigg), \qquad (18)
\end{aligned}$$

All second components are analogous by symmetry. The reset terms are defined in Eq. (3).

We do not have local conservative equality between the flux density across the threshold $(J^1_{\text{ind}}(v_{\text{th}}, v_2, t) + J^1_{\text{syn}}(v_{\text{th}}, v_2, t))$ and the reset $J_{\text{reset},1}(v_2, t)$. Due to our definition of the flux density $J^1_{\text{syn}}(v_{\text{th}}, v_2, t)$, it includes the effect of synchronous inputs where the voltage of neuron 2 jumps from v_2 to higher voltages (and hence appears in the reset term $J_{\text{reset},1}(v_2, t)$ at those higher voltage or even in $J_{\text{reset},3}(t)$ if neuron 2 also crossed threshold). Nonetheless, one can verify that the system is globally conservative because the total flux across threshold equals the total reset:

$$\begin{aligned}&\int_{v_{\text{reset}}}^{v_{\text{th}}} (J^1_{\text{ind}}(v_{\text{th}}, v_2, t) + J^1_{\text{syn}}(v_{\text{th}}, v_2, t))\mathrm{d}v_2 \\ &\quad + \int_{v_{\text{reset}}}^{v_{\text{th}}} (J^2_{\text{ind}}(v_1, v_{\text{th}}, t) + J^2_{\text{syn}}(v_1, v_{\text{th}}, t))\mathrm{d}v_1 \\ &\quad = \int_{v_{\text{reset}}}^{v_{\text{th}}} J_{\text{reset},1}(v_2, t)\mathrm{d}v_2 + \int_{v_{\text{reset}}}^{v_{\text{th}}} J_{\text{reset},2}(v_1, t)\mathrm{d}v_1 \\ &\quad + J_{\text{reset},3}(t) \end{aligned} \tag{19}$$

To numerically solve the equations, we used the finite volume approach. We discretized the domain $[0, v_{\text{th}}] \times [0, v_{\text{th}}]$ in (v_1, v_2) space into squares of size $\Delta v \times \Delta v$ with $\Delta v = 0.0125$. We let $v_{1,j} = v_{2,j} = (j - 1/2)\Delta v$ so that the point $(v_{1,j}, v_{2,k})$ is the center of square (j, k). Each point $\rho_{j,k}(t)$ represented the integral of $\rho(v_1, v_2, t)$ over the square (j, k). The divergence $\nabla \cdot \mathbf{J}$ at the center of each square was approximated by differences in the integral of the flux along the boundary of the square, and we approximated the resulting integrals along each line segment with the midpoint rule. We linearly interpolated $\rho_{j,k}$ to estimate its value along the boundary for J_{leak}. To estimate the value of the integrals for J_{ind} and J_{syn}, we used Simpson's rule.

We reduced the dimension of the system of equations by exploiting the symmetry $\rho_{j,k} = \rho_{k,j}$. We discretized in time using the trapezoid method with $\Delta t = 0.5$ ms. At each time step, we solved the system of linear equations using GMRES (Saad and Schultz 1986). In this way, we used a numerical method that is second order accurate in both time and space.

Since we set $v_{\text{reset}} < E_{\text{r}}$, the advection flux $\mathbf{J}_{\text{leak}}$ is non-zero along locations of voltage reset, preventing the $J_{\text{reset},1}$ and $J_{\text{reset},2}$ delta-function source terms from forming a delta-function in $\rho(v_1, v_2, t)$. However, the double delta-function source due to the reset $J_{\text{reset},3}$ will form a delta-function component of ρ. The flux $J_{\text{reset},3}$ represents a finite probability per unit time that both neurons reset to $(v_{\text{reset}}, v_{\text{reset}})$. At that point, the voltage pair will advect along the line $\{(v_1, v_2) | v_1 = v_2, 0 < v_1 < E_{\text{r}}\}$ until either neuron receives an input. Hence, there will be finite probability that the voltages of a neuron pair reside along this line. The delta-function in ρ along this line will prevent second order convergence of the above numerical method if we apply it directly to Eq. (17). To ensure convergence, we divide ρ into two components, a smooth component ρ_s and a delta function component along the diagonal with weight function ρ_δ:

$$\rho(v_1, v_2, t) = \rho_s(v_1, v_2, t) + \delta(v_1 - v_2)\rho_\delta(v_1) \tag{20}$$

Plugging this expression into the original evolution Eq. (17) and then grouping the delta-function terms will result in coupled evolution equations for ρ_s and ρ_δ. Since ρ_s and ρ_δ are smooth, we can solve the resulting equations using our numerical scheme and achieve second order accuracy.

B Calculating connectivity statistics for different network classes

We calculate the expected number of inputs W^1 and the fraction of shared inputs β for networks with arbitrary outgoing degree distributions and incoming connections determined randomly. We examine the connectivity from a presynaptic population 1 with N_1 neurons onto a postsynaptic population 2 with N_2 neurons.

Let $\hat{W}_{ij} = 1$ if there is a connection from neuron j in population 1 onto neuron i in population 2; otherwise, let $\hat{W}_{ij} = 0$. Let $d_j = \sum_{i=1}^{N_2} \hat{W}_{ij}$ be outgoing degree of neuron j in population 1, i.e., the number of connections from neuron j onto all neurons in population 2. Let the function $f(k)$ be the outgoing degree distribution so that

$$\Pr(d_j = k) = f(k)$$

for $k = 1, 2, \ldots, N_2$. The expected total number of connections (out of $N_1 N_2$ possible) is $N_1 \sum_{k=1}^{N_2} k f(k)$ so that the expected number of connections onto any neuron in population 2 is

$$W^1 = \frac{N_1}{N_2} \sum_{k=1}^{N_2} k f(k). \tag{21}$$

If $f(k)$ was given by a one-parameter family of distributions, prescribing W^1 would determine the particular distribution as a function of population sizes N_1 and N_2.

Neuron j in population 1 has d_j connections onto neurons in population 2, which we assume are assigned randomly to neurons in population 2. Then, conditioned on this value of d_j, the probability of a connection from neuron j onto any given pair (indexed by i_1 and i_2) of neurons in population 2 is

$$\Pr(\hat{W}_{i_1 j} = 1 \,\&\, \hat{W}_{i_2 j} = 1 \mid d_j) = \frac{\binom{N_2-2}{d_j-2}}{\binom{N_2}{d_j}} = \frac{d_j(d_j-1)}{N_2(N_2-1)}$$

Multiplying by the probability distribution of d_j (i.e., the outgoing degree distribution) and summing over all possible values of d_j, we determine that the probability a given neuron j in population 1 is connected to a given pair of neurons in population 2 is

$$\sum_{k=1}^{N_2} \Pr(\hat{W}_{i_1 j} = 1 \,\&\, \hat{W}_{i_2 j} = 1 \mid d_j = k) \Pr(d_j = k)$$

$$= \sum_{k=1}^{N_2} \frac{k(k-1)}{N_2(N_2-1)} f(k).$$

To calculate W^2, the total expected number of shared inputs from all N_1 neurons, we simply need to multiply by N_1:

$$W^2 = \sum_{k=1}^{N_2} \frac{N_1 k(k-1)}{N_2(N_2-1)} f(k).$$

Dividing by W^1 Eq. (21) gives the fraction of shared input parameter β in terms of the degree distribution

$$\beta = \frac{\sum_{k=1}^{N_2} k(k-1) f(k)}{(N_2-1)\sum_{k=1}^{N_2} k f(k)}. \tag{22}$$

For a random network, the degree distribution is a binomial distribution

$$f(k) = \binom{N_2}{k} p^k (1-p)^{N_2-k}$$

so that

$$W^1 = N_1 p \qquad \text{and} \qquad \beta = p, \tag{23}$$

agreeing with the results from Section 3.2.2. If the degree distribution is given by a power law with maximum degree $d_{\max} \le N_2$

$$f(k) = \begin{cases} k^{-\gamma} / \sum_{n=1}^{d_{\max}} n^{-\gamma} & \text{if } k \le d_{\max}, \\ 0 & \text{otherwise,} \end{cases}$$

the expressions for W^1 and β become

$$W^1 = \frac{N_1 \sum_{k=1}^{d_{\max}} k^{1-\gamma}}{N_2 \sum_{k=1}^{d_{\max}} k^{-\gamma}} \qquad \text{and}$$

$$\beta = \frac{\sum_{k=1}^{d_{\max}} (k-1) k^{1-\gamma}}{(N_2-1)\sum_{k=1}^{d_{\max}} k^{1-\gamma}}. \tag{24}$$

If the degree distribution is given by a Gaussian

$$f(k) = \frac{e^{-k^2/2\sigma^2}}{\sum_{n=1}^{N_2} e^{-n^2/2\sigma^2}}$$

the expressions for W^1 and β become

$$W^1 = \frac{N_1 \sum_{k=1}^{N_2} k e^{-k^2/2\sigma^2}}{N_2 \sum_{k=1}^{N_2} e^{-k^2/2\sigma^2}} \quad \text{and}$$

$$\beta = \frac{\sum_{k=1}^{N_2} k(k-1) e^{-k^2/2\sigma^2}}{(N_2-1)\sum_{k=1}^{N_2} k e^{-k^2/2\sigma^2}}. \tag{25}$$

In our simulations, we set $N_1 = N_2 = N$ and solved the first equation of Eq. (23), Eq. (24) or Eq. (25) for the p, γ or σ, respectively that gave the chosen W^1. Then,we used the second equation of Eq. (23), Eq. (24) or Eq. (25) to calculate β.

References

Abbott, L. F., & van Vreeswijk, C. (1993). Asynchronous states in networks of pulse-coupled oscillators. *Physical Review E.*, *48*, 1483–1490.

Apfaltrer, F., Ly, C., & Tranchina, D. (2006). Population density methods for stochastic neurons with realistic synaptic kinetics: Firing rate dynamics and fast computational methods. *Network: Computation in Neural Systems, 17*, 373–418.

Barna, G., Gröbler, T., & Érdi, P. (1998). Statistical model of the hippocampal CA3 region—II. The population framework: Model of rhythmic activity in the CA3 slice. *Biological Cybernetics, 79*, 309–321.

Binder, M. D., & Powers, R. K. (2001). Relationship between simulated common synaptic input and discharge synchrony in cat spinal motoneurons. *Journal of Neurophysiology, 86*, 2266–2275.

Brunel, N., & Hakim, V. (1999). Fast global oscillations in networks of integrate-and-fire neurons with low firing rates. *Neural Computation*, *11*(7), 1621–1671.

Cai, D., Tao, L., Rangan, A., & McLaughlin, D. (2006). Kinetic theory for neuronal network dynamics. *Communications in Mathematical Sciences*, *4*, 97–127.

Casti, A. R., Omurtag, A., Sornborger, A., Kaplan, E., Knight, B., Victor, J., et al. (2002). A population study of integrate-and-fire-or-burst neurons. *Neural Computation*, *14*, 957–86.

Câteau, H., & Fukai, F. (2001). Fokker–Planck approach to the pulse packet propagation in synfire chain. *Neural Networks*, *14*, 675–685.

Câteau, H., & Reyes, A. D. (2006). Relation between single neuron and population spiking statistics and effects on network activity. *Physical Review Letters*, *96*, 058, 101.

Diesmann, M., Gewaltig, M. O., & Aertsen, A. (1999). Stable propagation of synchronous spiking in cortical neural networks. *Nature*, *402*, 529–533.

Doiron, B., Rinzel, J., & Reyes, A. (2006). Stochastic synchronization in finite size spiking networks. *Physical Review E.*, *74*, 030, 903.

Dorn, J. D., & Ringach, D. L. (2003). Estimating membrane voltage correlations from extracellular spike trains. *Journal of Neurophysiology*, *89*, 2271–2278.

Galán, R. F., Fourcaud-Trocmé, N., Ermentrout, G. B., & Urban, N. N. (2006). Correlation-induced synchronization of oscillations in olfactory bulb neurons. *Journal of Neuroscience*, *26*, 3646–3655.

Gardiner, C. W. (2004). *Handbook of stochastic methods for physics, chemistry and the natural sciences,* 3rd edn. New York: Springer.

Gerstner, W. (2000). Population dynamics of spiking neurons: Fast transients, asynchronous states, and locking. *Neural Computation*, *12*, 43–89.

Hasegawa, H. (2003). Dynamical mean-field theory of spiking neuron ensembles: Response to a single spike with independent noises. *Physical Review E.*, *67*, 041, 903.

Haskell, E., Nykamp, D. Q., & Tranchina, D. (2001). Population density methods for large-scale modeling of neuronal networks with realistic synaptic kinetics: Cutting the dimension down to size. *Network: Computation in Neural Systems*, *12*(2), 141–174.

Hildebrand, E. J., Buice, M. A., & Chow, C. C. (2007). Kinetic theory of coupled oscillators. *Physical Review Letters*, *98*, 054, 101.

Hohn, N., & Burkitt, A. N. (2001). Shot noise in the leaky integrate-and-fire neuron. *Physical Review E.*, *63*, 031, 902.

Huertas, M. A., & Smith, G. (2006). A multivariate population density model of the dlgn/pgn relay. *Journal of Computational Neuroscience*, *21*, 171–89.

Ichimaru, S. (1973). Basic principles of plasma physics: A statistical approach. New York: Benjamin.

Jaynes, E. T. (1957). Information theory and statistical mechanics. *Physical Review*, *106*, 62–79.

Knight, B. W. (2000). Dynamics of encoding in neuron populations: Some general mathematical features. *Neural Computation*, *12*, 473–518.

Knight, B. W., Manin, D., & Sirovich, L. (1996). Dynamical models of interacting neuron populations. In E. C., Gerf, (Ed.), *Symposium on robotics and cybernetics: Computational engineering in systems applications, cite scientifique* Lille, France.

Litvak, V., Sompolinsky, H., Segev, I., & Abeles, M. (2003). On the transmission of rate code in long feedforward networks with excitatory-inhibitory balance. *Journal of Neuroscience, 23*, 3006–3015.

Ly, C., & Tranchina, D. (2008). Spike train statistics and dynamics with synaptic input from any renewal process: A population density approach. *Neural Computation*. doi:10.1162/neco.2008.03-08-743.

Masuda, N., & Aihara, K. (2002). Bridging rate coding and temporal spike coding by effect of noise. *Physical Review Letters*, *88*, 248, 101.

Mattia, M., & Del Giudice, P. (2002). Population dynamics of interacting spiking neurons. *Physical Review E.*, *66*, 051, 917.

McFadden, J. A. (1965). The entropy of a point process. *Journal of the Society for Industrial and Applied Mathematics*, *13*, 988–994.

Meffin, H., Burkitt, A. N., & Grayden, D. B. (2004). An analytical model for the "large, fluctuating synaptic conductance state" typical of neocortical neurons *in vivo*. *Journal of Computational Neuroscience*, *16*, 159–175.

Moreno, R., de la Rocha, J., Renart, A., & Parga, N. (2002). Response of spiking neurons to correlated inputs. *Physical Review Letters*, *89*, 288, 101.

Moreno-Bote, R., & Parga, N. (2006). Auto- and crosscorrelograms for the spike response of leaky integrate-and-fire neurons with slow synapses. *Physical Review Letters*, *96*, 028, 101.

Nicholson, D. (1992). *Introduction to plasma theory.* Malabar, Florida: Krieger.

Nirenberg, S., & Victor, J. (2007). Analyzing the activity of large populations of neurons: How tractable is the problem? *Current Opinion in Neurobiology*, *17*, 397–400.

Nykamp, D. Q. (2005). Revealing pairwise coupling in linear-nonlinear networks. *SIAM Journal on Applied Mathematics*, *65*, 2005–2032.

Nykamp, D. Q. (2007a). Exploiting history-dependent effects to infer network connectivity. *SIAM Journal on Applied Mathematics*, 68, 354–391.

Nykamp, D. Q. (2007b). A mathematical framework for inferring connectivity in probabilistic neuronal networks. *Mathematical Biosciences*, *205*, 204–251.

Nykamp, D. Q., & Tranchina, D. (2000). A population density approach that facilitates large-scale modeling of neural networks: Analysis and an application to orientation tuning. *Journal of Computational Neuroscience*, *8*, 19–50.

Nykamp, D. Q., & Tranchina, D. (2001). A population density approach that facilitates large-scale modeling of neural networks: Extension to slow inhibitory synapses. *Neural Computation*, *13*, 511–546.

Omurtag, A., Kaplan, E., Knight, B., & Sirovich, L. (2000a). A population approach to cortical dynamics with an application to orientation tuning. *Network: Computation in Neural Systems*, *11*, 247–260.

Omurtag, A., Knight, B. W., & Sirovich, L. (2000b). On the simulation of large populations of neurons. *Journal of Computational Neuroscience, 8*, 51–63.

Reyes, A. D. (2003). Synchrony-dependent propagation of firing rate in iteratively constructed networks *in vitro*. *Nature Neuroscience*, *6*, 593–599.

de la Rocha, J., Doiron, B., Shea-Brown, E., Josić, K., & Reyes, A. (2007). Correlation between neural spike trains increases with firing rate. *Nature*, *448*, 802–806.

de la Rocha, J., Moreno-Bote, R., & Câteau, H. (2008). *Propagation of temporally correlated spike trains: A Fokker-Planck analysis* (in preparation).

van Rossum, M. C. W., Turrigiano, G. G., & Nelson, S. B. (2002). Fast propagation of firing rates through layered networks of noisy neurons. *Journal of Neuroscience*, *22*, 1956–1966.

Saad, Y., & Schultz, M. H. (1986). GMRES: A generalized minimal residual algorithm for solving nonsymmetric linear systems. *SIAM Journal on Scientific and Statistical Computing*, *7*, 856–869.

Salinas, E., & Sejnowski, T. (2002). Integrate-and-fire neurons driven by correlated stochastic input. *Neural Computation*, *14*, 2111–2155.

Schneidman, E., Berry, M. J. II, Segev, R., & Bialek, W. (2006). Weak pairwise correlations imply strongly correlated network states in a neural population. *Nature*, *440*, 1007–1012.

Shadlen, M. N., & Newsome, W. T. (2001). Neural basis of a perceptual decision in the parietal cortex (area LIP) of the rhesus monkey. *Journal of Neurophysiology*, *86*, 1916–1936.

Shea-Brown, E., Josić, K., de la Rocha, J., & Doiron, B. (2008). Correlation and synchrony transfer in integrate-and-fire neurons: Basic properties and consequences for coding. *Physical Review Letters*, *100*, 108, 102.

Shinomoto, S., Shima, K., & Tanji, J. (2003). Differences in spiking patterns among cortical neurons. *Neural Computation*, *15*, 2823–2842.

Shlens, J., Field, G. D., Gauthier, J. L., Grivich, M. I., Petrusca, D., Sher, A., et al. (2006). The structure of multi-neuron firing patterns in primate retina. *Journal of Neuroscience*, *26*, 8254–8266.

Sirovich, L. (2008). Populations of tightly coupled neurons: The RGC/LGN system. *Neural Computation*, *20*, 1179–1210.

Sirovich, L., Knight, B., & Omurtag, A. (2000). Dynamics of neuronal populations: The equilibrium solution. *SIAM Journal on Applied Mathematics*, *60*, 2009–2028.

Sirovich, L., Omurtag, A., & Lubliner, K. (2006). Dynamics of neural populations: Stability and synchrony. *Network: Computation in Neural Systems*, *17*, 3–29.

Stevens, C., & Zador, A. (1998). Input synchrony and the irregular firing of cortical neurons. *Nature Neuroscience*, *1*, 210–207.

Svirskis, G., & Hounsgaard, J. (2003). Influence of membrane properties on spike synchronization in neurons: theory and experiments. *Network: Computation in Neural Systems 14*, 747–763.

Tang, A., Jackson, D., Hobbs, J., Chen, W., Smith, J. L., Patel, H., et al. (2008). A maximum entropy model applied to spatial and temporal correlations from cortical networks *in vitro*. *Journal of Neuroscience*, *28*, 505–518.

Wang, S., Wang, W., & Liu, F. (2006). Propagation of firing rate in a feed-forward neuronal network. *Physical Review Letters*, *96*, 018, 103.

Yu, S., Huang, D., Singer, W., & Nikolic, D. (2008). A small world of neuronal synchrony. *Cereb Cortex*. doi:10.1093/cercor/bhn047.